TRANSIENT SEISMIC VELOCITIES BENEATH ACTIVE VOLCANOES

by

Cody Kupres

A Thesis

Submitted to the Faculty of Purdue University

In Partial Fulfillment of the Requirements for the degree of

Master of Science

Department of Earth, Atmospheric, and Planetary Sciences

West Lafayette, Indiana

May 2024

THE PURDUE UNIVERSITY GRADUATE SCHOOL
STATEMENT OF COMMITTEE APPROVAL

Dr. Jonathan R. Delph, Chair

Department of Earth, Atmospheric, and Planetary Sciences

Dr. Xiaotao Yang

Department of Earth, Atmospheric, and Planetary Sciences

Dr. Michael Eddy

Department of Earth, Atmospheric, and Planetary Sciences

Approved by:

Dr. Daniel J. Cziczo

This thesis is dedicated to my parents. Mom and Dad, thank you for your support and encouragement throughout my academic journey. I love you both. And to my best friend, Josey. From every chewed-up sofa cushion to every morning awoo, you made every step of this journey worth it and it would not have been the same without you.

ACKNOWLEDGMENTS

I would like to thank my advisor and mentor, Dr. Xiaotao Yang, for his support and guidance throughout these last few years of my academic journey. His knowledge, patience, and dedication to our work have been invaluable, and I am grateful for the opportunity that I had to work with and learn from him.

I would also like to thank my committee members, Dr. Jonathon R. Delph and Dr. Michael Eddy, for their valuable insights and feedback.

Additionally, I would like to thank my collaborators who have contributed to my research projects in various capacities. I am thankful to Dr. Matt Haney at the Alaska Volcano Observatory, Dr. Diana C. Roman at the Carnegie Institution for Science, and Dr. Jeremy Maurer at Missouri University of Science and Technology for their collaboration, expertise, and support. Their contributions have greatly enhanced the quality and scope of my work, and I am grateful to have had the opportunity to work with such great people and scientists.

TABLE OF CONTENTS

LIST OF FIGURES

ABSTRACT

Volcanic eruptions provide crucial insights into the behavior of volcanic systems. Various eruption styles, surface deformation, and magma flux all play a role in how we interpret volcanic terrain. Yet our understanding of subsurface structural changes associated with the evolution of the eruption cycle, although essential for mitigating hazards and forecasting eruptions, remains limited. To address this issue, this thesis examined the seismic velocity changes at Great Sitkin Volcano (July 2019 to July 2023) and Okmok Volcano (July 2006 to July 2010) in the Aleutian volcanic arc. Employing single-station ambient noise interferometry to estimate changes in seismic velocity (dv/v), the results reported in this thesis provided significant insights into co-eruptive structural modifications. The seismic velocity changes were compared with complementary datasets, including seismicity and surface deformation, to develop a comprehensive understanding of the volcanic behavior. The dv/v results at Great Sitkin showed a sustained velocity increase coinciding with continued lava effusion following the initial explosive eruption on May 26, 2021. This was most prominent to the northwest of the summit caldera where seismic imaging revealed a potential magma reservoir. This spatially variable co-eruptive increase in seismic velocity was interpreted as reflecting the structural changes due to magma extrusion. The Okmok project investigated multiple phases of the eruption cycle associated with the July 12, 2008 eruption. Three distinct dv/v spikes were identified, including a co-eruptive spike and two post-eruptive spikes. These spikes were attributed to magma extrusion, reservoir depressurization, and subsequent episodes of magma recharge, causing surface deformation based on InSAR data analysis and earthquake activity. The findings from my research projects provided valuable insights into hazard mitigation and eruption forecasting at active volcanoes, by characterizing the complexity of magmatic systems with comprehensive co-eruptive structural modifications.

1. INTRODUCTION

Understanding the complexities of volcanic eruptions is important for mitigating their potential hazards and societal impacts. Volcanic eruptions exhibit diverse eruption styles, durations, and observable precursors, posing significant scientific challenges (National Academies of Sciences and Medicine, 2017; Orr et al., 2024). To improve eruption prediction and hazard assessment, it is essential to gain a comprehensive understanding of the dynamics of magmatic activity, encompassing magma transport and eruptive behaviors across different spatial (ranging from meters to tens of kilometers) and temporal (spanning from days to years) scales (Brown et al., 2015).

Monitoring temporal changes in seismic velocity (dv/v) is an increasingly popular tool in studying volcanic eruptions, offering insights into magma dynamics and associated hazards (Bennington et al., 2018; Brenguier et al., 2008; Donaldson et al., 2019; Feng et al., 2020; Olivier et al., 2019; Ruiz et al., 2022). This thesis reviews the findings of two research projects that utilize the same methodology at two different volcanoes with distinct eruptive cycles.

Chapter 2 summarizes the method and workflow for measuring seismic velocity changes using single-station interferometry. It compares the dv/v results of the cross-component and same-component correlation functions and also shows the testing results using different coda wave window lengths at multiple frequencies. This chapter provides a methodological background for Chapters 3 and 4.

Chapter 3 reports the research results at Great Sitkin Volcano. This research has been submitted to Geophysical Research Letters and is currently under review. The text is mostly from the submitted manuscript, reformatted for this thesis. This paper, titled "Sustained co-eruptive increase in seismic velocity below Great Sitkin Volcano due to magma extrusion", explores the significant increases in seismic velocity observed during the continued 2021 eruption of Great Sitkin Volcano. Remote volcanoes, such as the Great Sitkin Volcano in the central Aleutian volcanic arc, often have limited monitoring networks, stressing the importance of innovative approaches, like single-station seismic velocity monitoring, in un-

derstanding their behavior. This study provides insights into the dynamics of Great Sitkins complex magma transport and eruption processes.

Chapter 4 reports the dv/v results at Okmok Volcano, compared with surface deformation. The manuscript on this research is in preparation. This paper, tentatively titled "Transient seismic velocity changes at Okmok Volcano reveal episodes of magma discharge and recharge", delves into the eruptive cycle of Okmok Volcano, spanning pre-, co-, and post-eruption phases. The dv/v analysis was compared with InSAR deformation data. Building upon the frameworks established in the first paper, this study offers a comprehensive analysis of seismic velocity changes, during a more complete eruption cycle of Okmok Volcano.

Chapter 5 summarizes the conclusion of the two research projects. By integrating the insights we learned from these two papers, this thesis provides a framework for the interpretation of changes in seismic velocity (dv/v) beneath active volcanic systems by drawing from the insights of the eruptive cycles at Great Sitkin and Okmok Volcanoes. This interdisciplinary approach of combining seismic and geodetic data and methods helped to advance our understanding of volcanic processes and enhance volcanic monitoring and hazard assessment practices.

2. DATA AND METHODS

This chapter summarizes the data and methods for measuring seismic velocity changes, as reported in Chapters 3 and 4. For Chapter 4, the *dv/v* results were compared with surface deformation from InSAR analysis. For consistency and completeness, this chapter also briefly introduces the processing steps and parameters for the InSAR analysis, conducted by collaborator Dr. Jeremy Maurer for the Okmok project.

2.1 Continuous seismic waveforms

We utilized a similar methodology to estimate transient seismic velocity changes (*dv/v*) beneath both Great Sitkin and Okmok Volcanoes. For Great Sitkin Volcano, five three-component broadband seismometers, operated by the Alaska Volcano Observatory (network code: AV; Alaska Volcano Observatory/USGS, 1988), were deployed on Great Sitkin Island (Figure 3.1a). The stations included GSCK, GSMY, GSSP, GSTD, and GSTR. We collected three-component continuous seismic waveforms from June 2019 to July 2023 from all stations. At Okmok Volcano, vertical-component seismic records from nine short-period seismometers operated by the Alaska Volcano Observatory (network code: AV; Alaska Volcano Observatory/USGS, 1988) were used on Umnak Island (Figure 4.1). Three broadband seismometers were excluded from the analysis due to insufficient data coverage. Continuous seismic waveforms of the Z-component were downloaded from July 2006 to July 2010 from all nine stations. Due to relatively sparse station coverage, we adopted a single-station approach to estimate seismic velocity variations (De Plaen et al., 2016. This involved computing single-station cross-component (XC) correlations and single-station same-component (SC) correlations, or auto-correlations. The methodology for ambient noise correlations and *dv/v* calculations utilized the *SeisGo* package (Yang et al., 2022a, 2022b).

2.2 Estimates of transient velocity changes

The continuous waveforms were initially sliced into 2-hour segments with a 1-hour overlap. Subsequently, noise correlation functions (NCF) were normalized using a frequency-time

normalization method (Shen et al., 2012). NCF computation was conducted for six correlation component pairs (EE, NN, ZZ, EZ, NZ, and EN), and short-term NCFs were stacked every 12 hours using the robust stacking method (Yang et al., 2022b). We measured dv/v using the trace stretching method (Sens-Schönfelder and Wegler, 2006; Yuan et al., 2021) in four frequency bands (0.1-0.4, 0.4-1, 1-2, and 2-3 Hz) to ensure the stability of the results. The dv/v measurements were averaged across all component pairs within each frequency band (Figure 2.4. Our analysis is primarily focused on the 1-2 Hz, a frequency range that is sensitive to volcanic activity in the shallow crust (Cubuk-Sabuncu et al., 2021; De Plaen et al., 2016).

At Great Sitkin, the reference trace for dv/v measurement was robustly stacked NCFs from June 2019 to February 2020, a period of relatively low seismic activity. At Okmok, the reference trace was derived from stacked NCFs from July 2006 to June 2007, which was a period of low seismic activity at the volcano. Additionally, at Okmok, geodetic InSAR data from the Advanced Land Observation Satellite (ALOS) was utilized. At both volcanoes, the dv/v calculations were compared with earthquakes from the USGS Comprehensive Catalog (U.S. Geological Survey, 2022).

2.3 Evaluate the effect of coda window length

The coda window represents the portion of the seismic waves resulting from subsurface scattering following the main arrival in the noise correlation function. The choice of the time window within the coda wave for dv/v measurements was carefully considered, with a window length of 1-13s selected for both volcanoes based on convergence of results (Luo et al., 2023). To examine the effects of the length of the coda window on the estimates of seismic velocity changes (dv/v), we conducted a series of tests to measure the dv/v values with varying coda window lengths (Figure 2.1 and 2.2). The tests revealed that the dv/v values gradually converge with increasing coda window length, eventually reaching a plateau at a specific time.

At Great Sitkin Volcano, the cross-component correlations exhibited a decrease in the rate of change with extended coda window lengths (Figure 2.2). Typically, the rate of

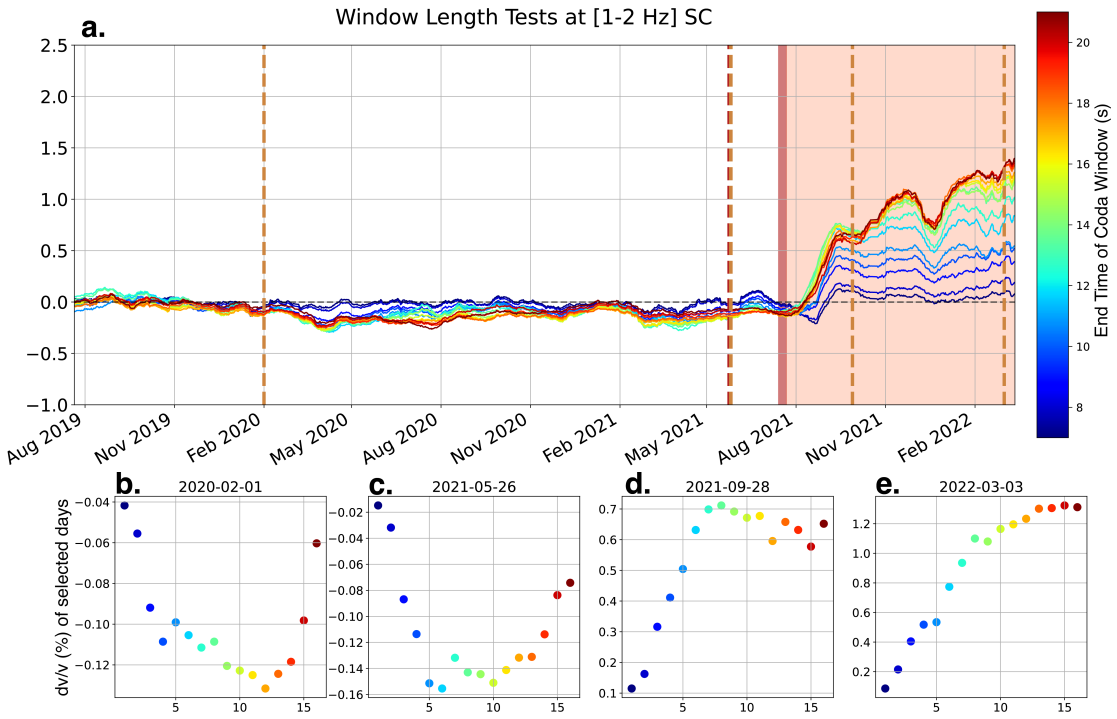

Figure 2.1. Comparison of SC dv/v result with varying coda window lengths. (a) All dv/v results from August 2019 to March 2022. Lines are color-coded by the ending time of the coda window from 7 s to 21 s, with the same starting time (1 s). (b-e) dv/v results for selected individual days, indicated by vertical dashed lines in (a).

change between different lengths began to taper around 5 to 7 seconds, indicating the coda window's ability to capture relevant seismic velocity changes earlier in the scattering process. In contrast, the same-component correlation results showed a peak (Figure 2.1b-e) at around 11 to 13 seconds into the coda wave, suggesting its ability to capture seismic velocity changes later in the coda window.

To ensure consistency and capture the maximum dv/v, we selected a coda window length of 13 seconds for all dv/v calculations in our studies. This choice was based on the convergence of dv/v values observed across different coda window lengths and the ability of the selected window length to capture seismic velocity changes at various times in the scattering process.

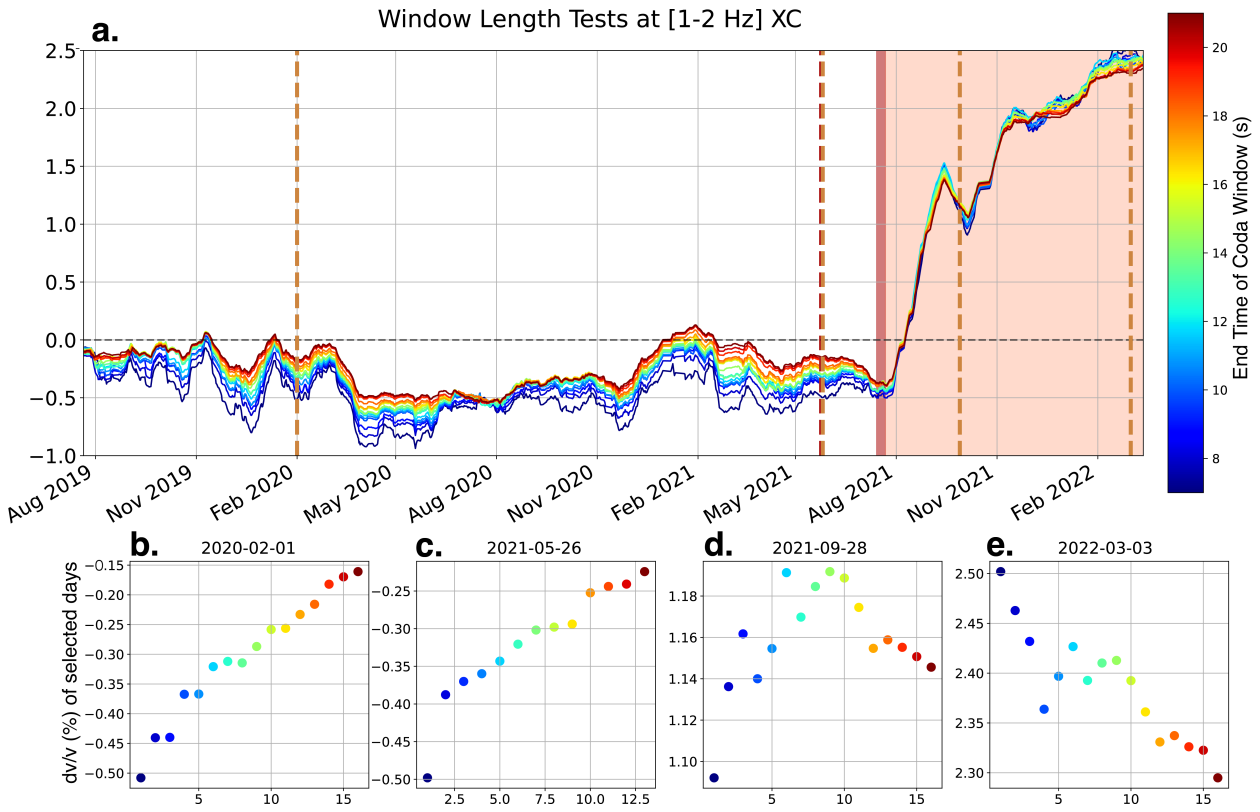

Figure 2.2. Comparison of XC *dv/v* result with varying coda window lengths. (a) All *dv/v* results from August 2019 to March 2022. Lines are color-coded by the ending time of the coda window from 7 s to 21 s, with the same starting time (1 s). (b-e) *dv/v* results for selected individual days, indicated by vertical dashed lines in (a).

2.4 Surface deformation from InSAR analysis

For comparison, we also processed remote sensing data from ALOS-PALSAR to obtain the displacement time series for Okmok. We downloaded single-look complex SAR images acquired in the stripmap mode for ascending track 300 from the Alaska Satellite Facility and processed them with the *stackStripMap.py* application in the InSAR Scientific Computing Environment software package (Rosen et al., 2012). The stack was geometrically registered to the acquisition acquired on February 17, 2007. We performed regular interferometric processing to make interferograms and coherence maps. We then applied topography-related phase components corrections to the interferograms using the 30 m resolution SRTM DEM

(Farr et al., 2007). This was followed by unwrapping the interferograms using the statistical Minimum Cost Flow algorithm (Chen and Zebker, 2002; Chen and Zebker, 2001). We used the Mintpy processing software (Yunjun et al., 2019) to convert the interferograms to time series.

We did not apply a tropospheric correction to the time series data due to the poor performance of the ERA-5 weather model in this region. However, we applied a linear deramping and topographic correction. The deformation is relative to GNSS site AB02 about 60 km southwest of the Okmok caldera center. From the InSAR deformation images at different time stamps, we extracted the time series of surface deformation, as displacements, at the corresponding seismic stations for comparison with the dv/v results.

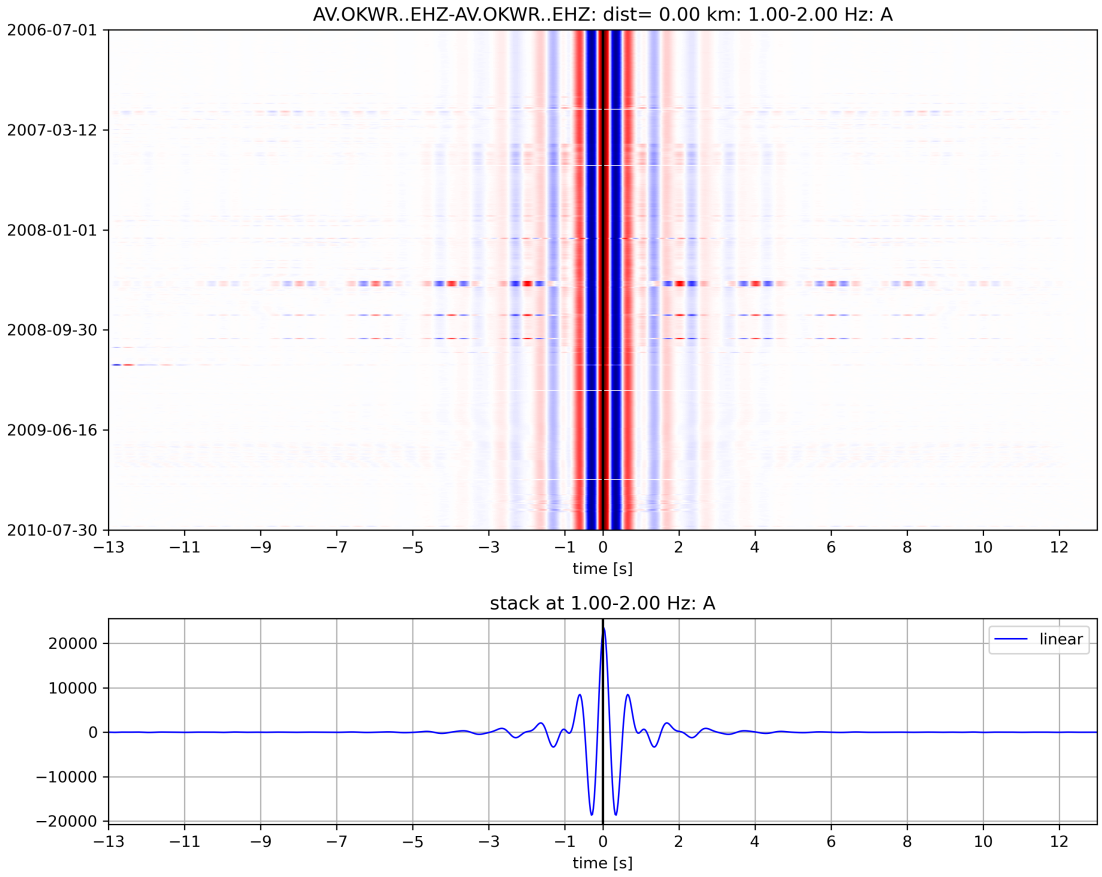

Figure 2.3. Example of single-station same-component NCFs at station AV.OKWR. The top panel shows NCFs of the vertical components filtered at 1.0-2.0 Hz, stacked over 3-day windows. The bottom panel shows a stack of all the NCFs.

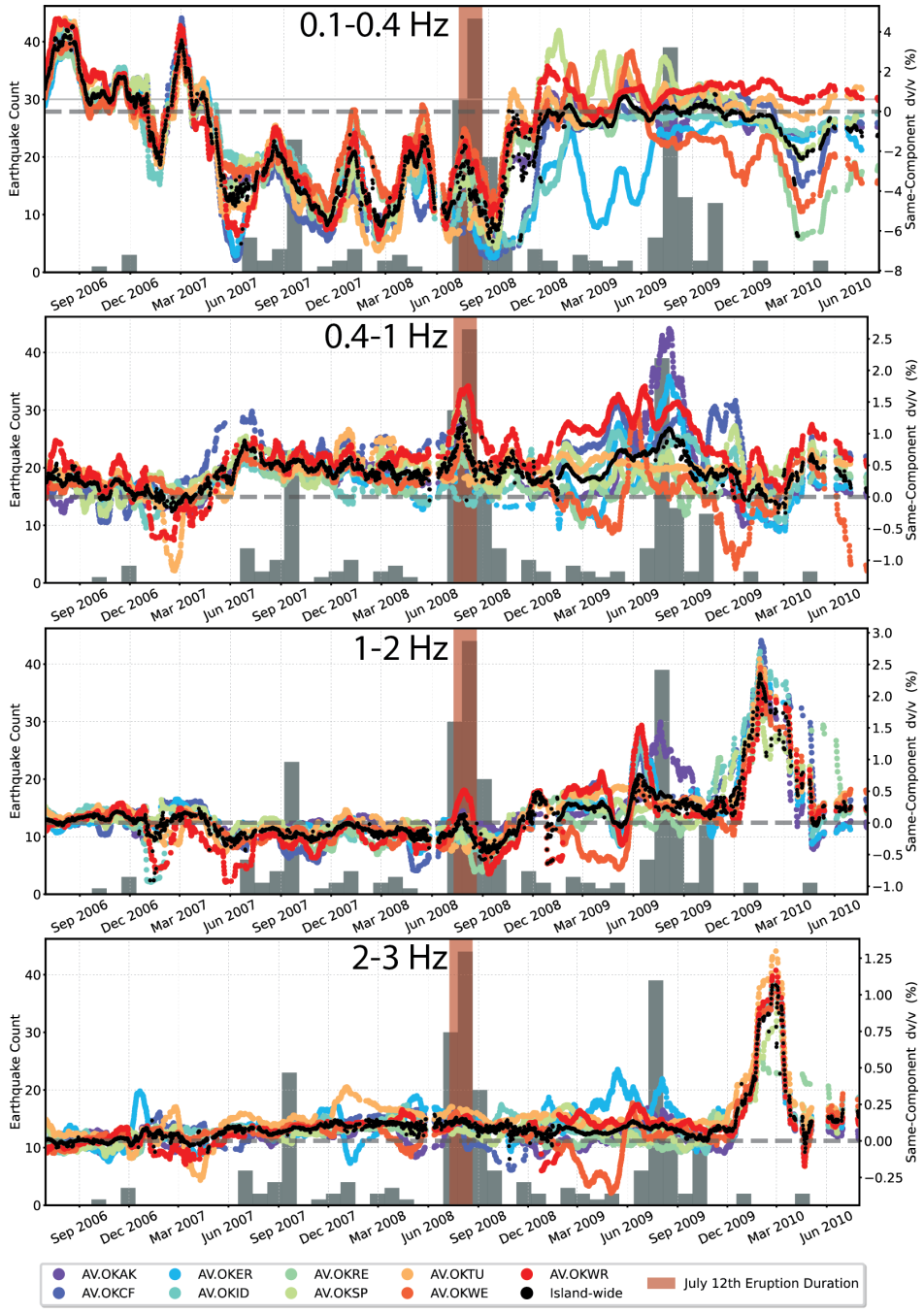

Figure 2.4. Estimates of *dv/v* from Z-component autocorrelation at different frequencies. The frequency bands tested include 0.1-0.4 Hz, 0.4-1 Hz, 1-2 Hz, and 2-3 Hz. For visualization, we smooth the dv/v time-series data using a 20-day moving window average. The grey histogram shows the earthquake count around Okmok Volcano from the USGS ComCat catalog. The July 2008 eruption is denoted by the red region. The time range used to create the reference trace for *dv/v* analysis is shaded in grey.

3. SEISMIC VELOCITY CHANGES AT GREAT SITKIN VOLCANO

*Note: This chapter is a manuscript currently under review in Geophysical Research Letters. The text has been reformatted to meet the thesis requirement. The data and methods section, as well as the supplementary materials, have been merged with Chapter 2 of this thesis. The manuscript is coauthored by Xiaotao Yang (Department of Earth, Atmospheric, and Planetary Sciences, Purdue University), Matt Haney (U.S. Geological Survey, Alaska Volcano Observatory), and Diana C. Roman (Earth and Planets Laboratory, Carnegie Institution for Science).

Below is the citation information for this manuscript:

Kupres, C. A., Yang, X., Haney, M., & Roman, D. C. (in review). Sustained co-eruptive increase in seismic velocity below Great Sitkin volcano due to magma extrusion. *Geophysical Research Letters*.

3.1 Introduction

Great Sitkin Volcano, located in the Aleutian Islands, is characterized by its recent significant volcanic unrest, culminating in the 2021 eruption. The eruption, preceded by a phreatic event in 2018, began explosively in May 2021, followed by a transition to effusive activity. Ongoing seismicity and the emplacement of a lava dome have characterized the post-eruptive period. Recent studies have proposed a complex magmatic system beneath Great Sitkin, with implications for eruption dynamics. In this chapter, we aim to investigate the multifaceted aspects of the 2021 eruption cycle of Great Sitkin by examining dv/v variations. Our research seeks to elucidate the magma dynamics, eruption evolution, and associated seismicity through detailed analysis of seismic velocity changes.

Great Sitkin Volcano, with a peak elevation of 1740 m, occupies the majority of the northern side of the island. The volcano features a summit crater and a lava dome that was emplaced during an eruption in February 1974 (Waythomas et al., 2003a). The 1974 eruption was the last eruption before the May 26, 2021, explosive eruption which lasted for 1-2 minutes (Alaska Volcano Observatory, 2021a; Bishop et al., 2023; Dietterich et al., 2023), except for a phreatic eruption in June 2018. The explosive eruption was followed by a two-month quiet period before the onset of the continuing effusive eruption and the emplacement of a lava dome since late July 2021 (Alaska Volcano Observatory, 2021b; Dietterich et al.,

2023; Haney et al., 2022a, 2022b). By September 2021, the lava dome bordered the crater rim and began to overflow the south and west caldera walls (Global Volcanism Program, 2021). As of July 2023 (the end of our observational period), the volcano continued to erupt effusively and the lava flow field grew ever larger (Global Volcanism Program, 2023). Local earthquakes are concentrated within an NW-SE zone, shallowest below the caldera (Figure 3.1b). Yang et al. (2023) propose a magmatic system consisting of two magma reservoirs to the northwest and southeast of the crater, to explain the distribution and spatiotemporal migration of the seismicity across the island.

The unrest at Great Sitkin has garnered significant interest in recent studies (Dietterich et al., 2023; Haney et al., 2022b; Pesicek et al., 2008; Power et al., 2004; J. Wang et al., 2023; Yang et al., 2023). The recent full-wave ambient noise tomography work at Great Sitkin (Yang et al., 2023) suggested two distinct magma reservoirs, leading to a hypothesis

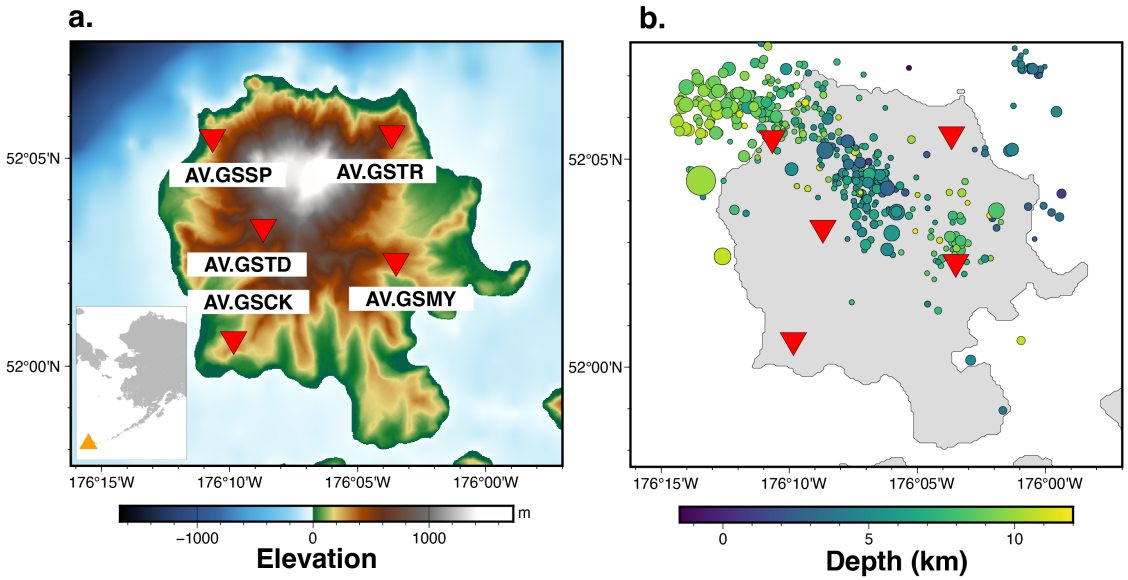

Figure 3.1. Seismic stations and seismicity at Great Sitkin Island. (a) Distribution of seismic stations (inverted red triangles) used in this study. (b) Earthquakes (magnitude ≥1) between January 2021 and January 2023 from USGS Comprehensive Earthquake Catalog (ComCat) (U.S. Geological Survey, 2022). The earthquakes are color-coded by the depths and scaled by the magnitudes.

of a complex six-stage eruption cycle for the ongoing 2021 eruption. By examining the changes in seismic velocities (dv/v) at Great Sitkin, we aim to enhance our understanding of how the subsurface structure of the volcanic system evolves throughout different stages of the eruption cycle. The investigation of dv/v at Great Sitkin provides an opportunity to monitor volcanoes with limited seismic data and characterize the behavior of complex volcanic systems.

In this study, we characterize the variation of seismic velocities (dv/v) from June 2019 to July 2023 at five seismic stations at Great Sitkin. We integrate dv/v measurements with observations of eruptive behaviors, seismicity, and a shear-wave velocity model (Yang et al., 2023) to delineate the magma dynamics and the eruption cycle of Great Sitkin Volcano. We observe a long-term co-eruptive increase in seismic velocity, likely induced by magma extrusion, most prominently at the station (GSSP) above a possible major magma reservoir northwest of the caldera. Our findings indicate that the dv/v at Great Sitkin primarily reflects magmatic extrusion from the reservoir and the subsequent co-eruptive processes, such as the deflation of the volcano, closure of cracks, and reduced melt content in the reservoir.

3.2 Results

The XC and SC dv/v measurements exhibit a similar overall pattern, characterized by short-term variations before a substantial increase in late July 2021 followed by minimal fluctuations at the elevated level (Figure 3.2). The velocity changes from the cross-component results (Figure 3.2a) exhibit larger amplitudes compared to the same-component results (Figure 3.2b). The dv/v before the onset of lava effusion in late July 2021 varies in the range of -0.6% to 0.75% and -0.3% to 0.4% in the XC and SC results, respectively. The significant velocity increase that began in late July 2021 is most prominent at GSSP (Figure 3.2a-b), with a value of about 2.5% and 1% to 2% from the XC and SC results, respectively (Figure 3.2d). By approximately March 2022, all stations have reached maximum dv/v, with only minor variations within $\pm$0.25% around the elevated levels. The increase in velocity since late July 2021 coincides with an abrupt drop in eruptive seismicity (Figure 3.2c-d).

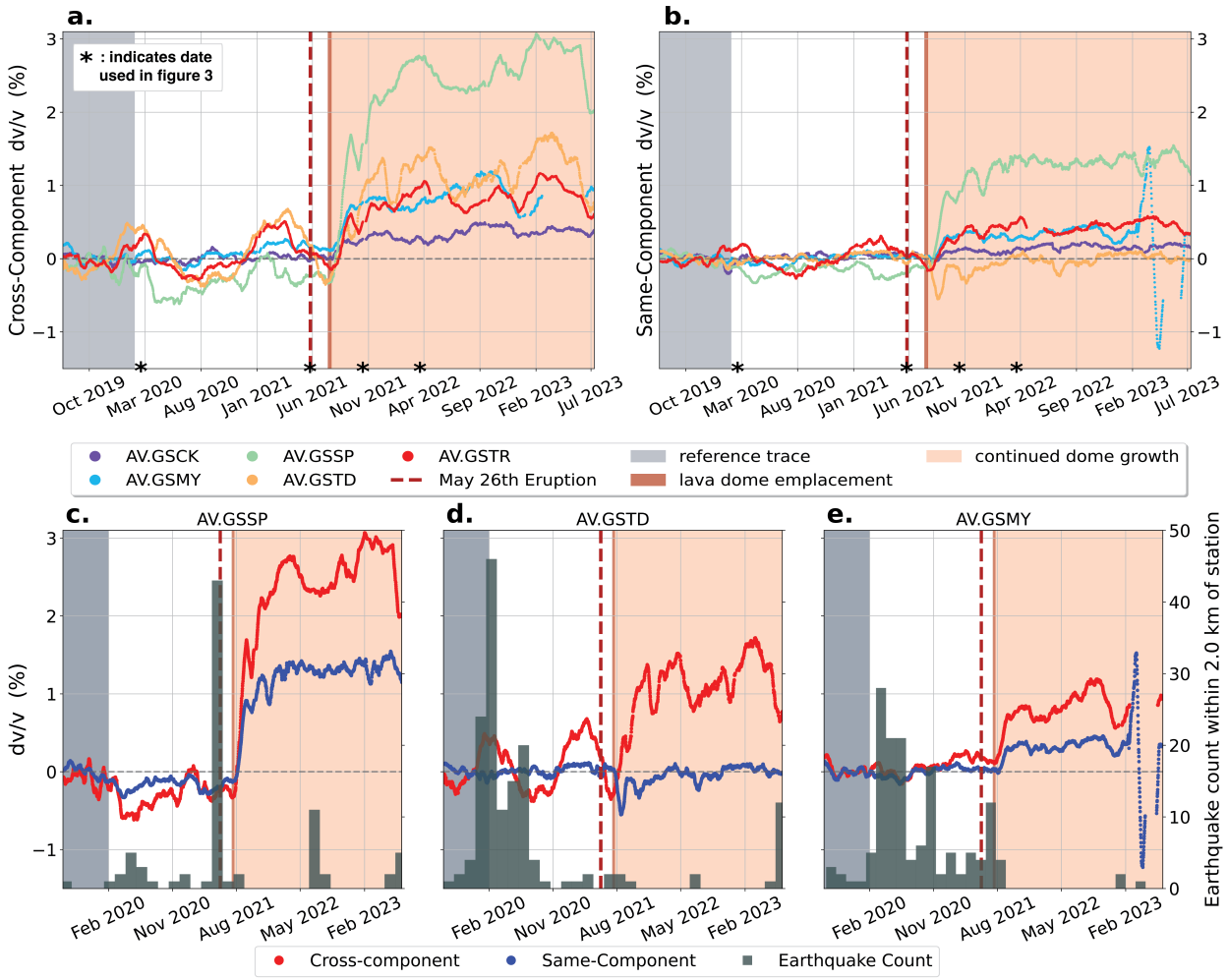

Figure 3.2. Estimates of *dv/v* for both the cross-component (XC) and same-component (SC) NCFs. (a-b) Station-average *dv/v* for XC and SC data, respectively. When plotting, we smooth the dv/v time-series data using a 20-day moving window average. The asterisks along the bottom of the y-axis denote the dates selected for use in Figure 3.3 and Supplementary Figures S1-S3. (c-e) Comparison of XC and SC results at stations GSMY (c), GSSP (d) and GSTD (e). For reference, we show the local seismicity with epicentral distances less than 2 km from the station above the depth of 12 km (dark green shaded bars). The explosive eruption is labeled by the red dashed line. The effusive lava flow period is marked by the orange-shaded area. The gray-shaded area denotes the time range used to produce the reference trace for *dv/v* analysis.

From March to June 2023, station GSMY shows a large fluctuation in *dv/v* in the SC results

and a gap in the XC results due to poor quality of the raw data (Figure 3.2c). This fluctuation is a consequence of an instrumental failure.

The largest increases in seismic velocity coincide with the low shear-wave velocity anomalies imaged by Yang et al. (2023) across the island from NW to SE as seen in Figure 3.3 where the XC *dv/v* measurements are compared with the shear-wave velocity structure from

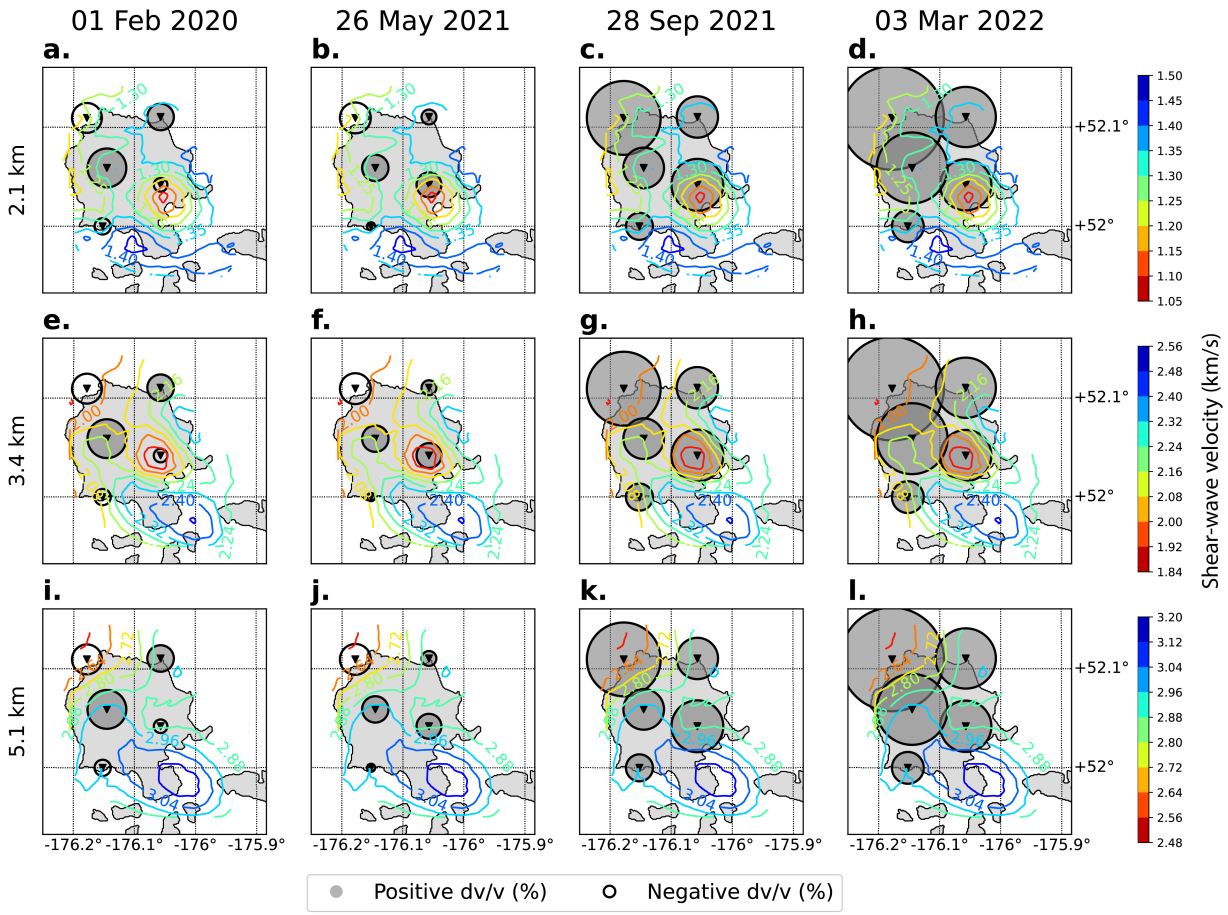

Figure 3.3. Comparison of cross-component *dv/v* results (circles) at different times with the shear wave velocities (color-coded contours) at different depths. From left to right are the *dv/v* on 1 Feb 2020, 26 May 2021, 28 Sep 2021, and 3 Mar 2022, respectively. The size of the circles around each station is scaled by their absolute *dv/v* value, disregarding the signs. Negative and positive dv/v values are in unfilled and filled circles, respectively. From top to bottom are the shear-wave velocities at the depths of 2.07, 3.42, and 5.11 km, respectively. The color range of the shear-wave velocity contours is the same for the same depth, with red indicating lower velocity and blue indicating higher velocity.

Yang et al. (2023). The shear-wave velocity model shows two low-velocity anomalies, with one to the southeast of the volcano edifice above a depth of about 4 km and a larger one to the northwest of the volcano edifice at a depth of >3 km (Yang et al., 2023). The alignment of these two low-velocity anomalies, interpreted as magma reservoirs by Yang et al. (2023), are correlated with the distribution of earthquakes along the NW-SE trending zone (Figure 3.1). Co-eruption, the largest velocity increases are estimated at stations broadly located along the NW-SE oriented zone of lower seismic velocities, but most dramatically to the northwest. This correlation is most prominently shown in the velocity distribution at 3.4 km (Figure 3.3g and h). The subsurface seismic velocity displays a pronounced transition from small pre-eruptive negative dv/v to larger co-eruptive positive dv/v, as shown in Figure 3.2.

3.3 Discussion

3.3.1 Key factors driving velocity changes at Great Sitkin

We observe a distinct increase in seismic velocity during the lava effusion since late July 2021 at Great Sitkin Volcano. Since the onset of lava effusion, the removal of magma from the subsurface, together with the consequent decrease in pressure, can cause deflation of the volcano (Peltier et al., 2010; J. Wang et al., 2023) and the closure of cracks that were propped open by high pressures in the reservoir within the medium (Duputel et al., 2009; Rivet et al., 2014; Sens-Schönfelder et al., 2014). This would effectively reduce the pore space below the volcano and the melt percent within the magmatic plumbing system (Figure 3.4), leading to an increase in seismic velocities. This is the opposite process of what several studies have suggested that inflation of the volcano would cause a decrease in velocity or a negative dv/v (Cubuk-Sabuncu et al., 2021; Olivier et al., 2019). A recent study from Wang et al. (2023) that used InSAR data revealed the inflation of Great Sitkin Volcano. Inflation started in September 2018 and peaked in September 2020, followed by a rapid co-eruptive deflation in October 2021. They suggest that the inflation resulted from magma accumulation within the reservoir and the subsequent deflation is a consequence of the continued lava effusion. While all of the aforementioned co-eruptive processes could independently cause the increase

of seismic velocity, we currently lack a method to narrow them down, so each must be taken into consideration.

During effusive eruptions, the movement of magma from the reservoir to the surface reduces the melt content within the reservoir, leading to an increase in its seismic velocities. Magma reservoirs, with partial melts, are commonly imaged as low seismic velocities (Delph et al., 2017; Lees, 2007; D. Miller et al., 2020; Paulatto et al., 2022). As melt-rich magma is extruded and transported, the reservoir experiences a reduction in melt percent.(Paulatto et al., 2022). This shift in melt percent directly affects the seismic velocity, with higher velocities expected for magmas with lower melt percentages.

The contribution of earthquake damage to seismic velocity changes at Great Sitkin seems to be negligible based on the lack of clear correlation between the seismicity rate and dv/v. To examine earthquake-induced changes in seismic velocity as in Lesage et al. (2014); Olivier et al. (2019), we compare the XC and SC dv/v with local seismicity around each station (histograms in Figure 3.2c-e), based the preliminary earthquake locations from the USGS ComCat (U.S. Geological Survey, 2022). We focus on stations GSMY, GSSP, and GSTD along the NW-SE alignment of the imaged magma reservoirs (Yang et al., 2023) and the concentration of eruptive seismicity (Figure 3.1b). During the time encapsulating the explosive eruption period (5/1/2021 to 6/1/2021), the largest recorded earthquake has a magnitude of 1.6. The earthquakes are likely too small to cause significant changes in seismic velocities, as the resultant structural damage would be relatively negligible (Olivier et al., 2019). This explains the lack of abrupt velocity drop even during the peak seismicity swarm on the day of the explosive eruption (May 26, 2021), when the observed dv/v values remained within the range of the background level. In contrast, the drastic increase in dv/v is correlated with the onset of the effusive eruption and the subsequent formation of the lava dome (Dietterich et al., 2023). The onset of the effusive eruption is coincident with a drop in seismicity. This correlation indicates that magma extrusion plays a more dominant role than earthquakes in influencing the co-eruptive seismic velocities at Great Sitkin.

3.3.2 Absence of pre-eruptive velocity decrease

At Great Sitkin, there is no detectable pre-eruptive decrease in seismic velocity as observed at several other volcanoes. The dv/v exhibits minor decreases at some stations (GSSP, GSTD, and GSTR) before the onset of the effusive eruption, however, observed decreases are not outside minor background variation levels and, as such, should not be characterized as distinct precursory drops. Notable eruptions that featured a distinct dv/v decrease include the 2018 Kilauea eruption (Olivier et al., 2019) and the 2010 and 2014 Piton de la Fournaise eruptions (De Plaen et al., 2016; Sens-Schönfelder et al., 2014). It is important to note, however, that Kilauea and Piton de la Fournaise are basaltic shield volcanoes at hotspots and not a subduction zone stratovolcano like Great Sitkin. These other eruptions were also accompanied by larger earthquakes than what was observed at Great Sitkin, which is known to correlate with velocity decreases (Wegler et al., 2009) interpreted as increasing permeability or formation of cracks beneath the volcano (Lesage et al., 2014).

We argue that the abrupt precursory velocity drop observed elsewhere is primarily due to seismic activity, as proposed by Olivier et al. (2019), instead of changes in magma (recharge/extraction). As discussed earlier, earthquake damage plays a minor role in the observed velocity changes at Great Sitkin. We argue that the lack of large pre-eruptive earthquakes at Great Sitkin could explain why a precursory decrease in seismic velocity is not detected.

3.3.3 Hypotheses for the sustained co-eruptive velocity increase

The increase in seismic velocity following the start of the lava effusion continues to at least the end of our observation period (July 2023), representing a long-term rather than transient change. We propose that magmatic activity has induced a persistent structural alteration beneath Great Sitkin relative to its pre-eruptive structure. We consider two end-member hypotheses to explain the sustained co-eruptive increase in seismic velocity, predominantly to the northwest of the crater (Figure 3.4). Hypothesis-1 suggests that the change in melt content and the closure of cracks around the reservoirs cause the velocity increase. Hypothesis-2 suggests the closure of shallow cracks within the volcaniclastics on the northwestern flank

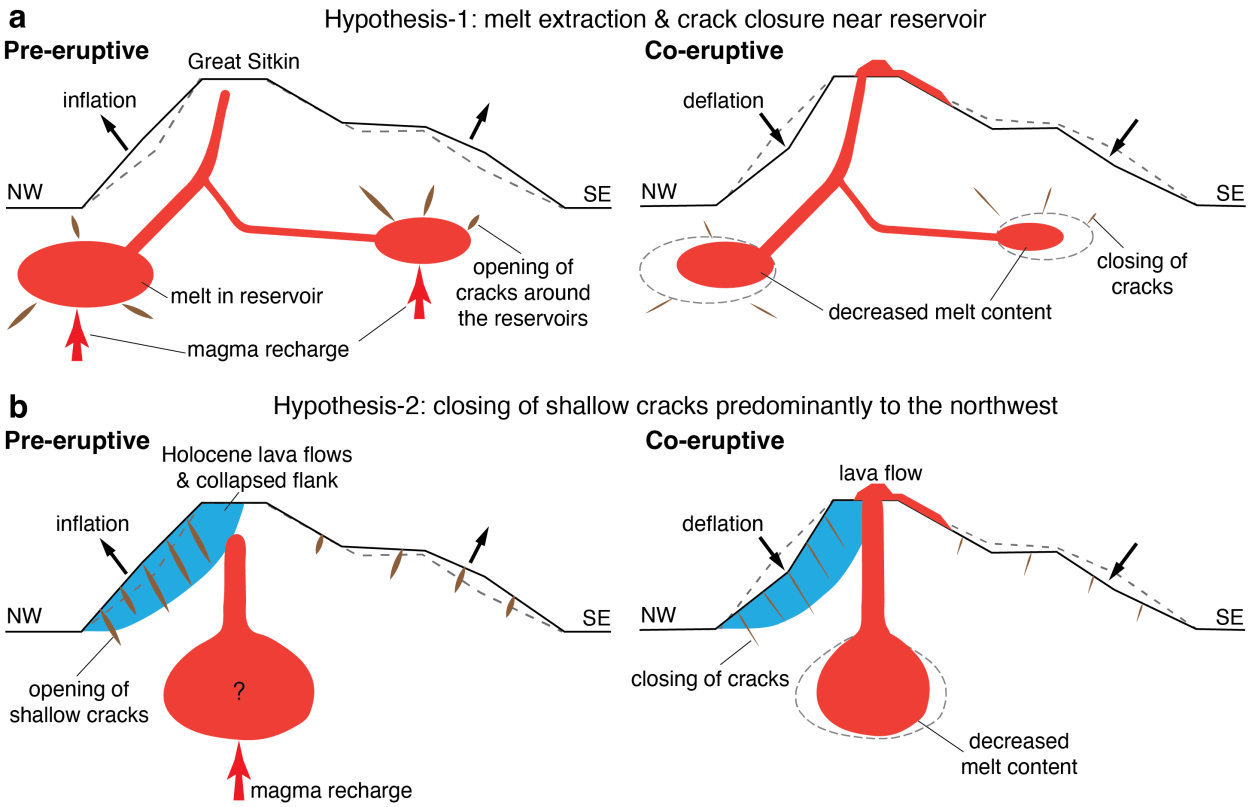

Figure 3.4. Diagrams illustrating the two hypotheses at Great Sitkin Volcano for the sustained co-eruptive seismic velocity increase, predominantly to the northwest of the caldera. (a) Hypothesis-1: The change in melt content and the closure of cracks around the reservoirs cause the velocity increase. (b) Hypothesis-2: The closure of shallow cracks within the volcaniclastics causes the velocity increase. The diagram on the left of each panel shows the pre-eruptive inflation of the volcano with the accumulation of melt within the magma reservoirs and the opening of cracks. The diagrams on the right are the co-eruptive processes (melt extraction, closing of cracks, and deflation) responsible for the observed increase in seismic velocity. Major features in these diagrams are not to scale.

causes the velocity increase. In practice, the co-eruptive subsurface structural variations and the cause of the velocity increase may be a combination of these two hypotheses.

Hypothesis-1: velocity increase due to melt extraction and closing of cracks near the reservoir (Figure 3.4a). In this hypothesis, the velocity increase is dominantly caused by processes within and close to the magma reservoir. Yang et al. (2023) proposes a double-

reservoir magmatic system below Great Sitkin to the northwest and southeast of the caldera, where two low shear-wave velocity anomalies are imaged (Figure 3.3). The reservoir to the northwest is larger and deeper than the one to the southeast (Yang et al., 2023). We attribute the different amplitudes of velocity increase to the difference in melt extraction, pressurization, and cracks around the two reservoirs. Velocity increase due to the decrease of melt content has been proposed before to explain similar long-term velocity increases documented at other volcanoes (Donaldson et al., 2019; Duputel et al., 2009).

The location with the largest velocity increase correlates with the distribution of low shear-wave velocity anomalies associated with the two interpreted magma reservoirs (Figure 3.3; Yang et al., 2023). This correlation is particularly prominent at 3.4 km after the lava effusion started (Figure 3.3g and h). The co-eruptive increase of dv/v provides additional and independent support for active magmatic movements, predominantly beneath the northwest region of the island and lesser activity to the southeast. The relatively larger co-eruptive increase in seismic velocity at GSSP compared to other stations suggests sustained magma supply primarily from the northwestern magma reservoir.

Hypothesis-2: velocity increase due to the closing of cracks within the shallow volcaniclastics (Figure 3.4b). A similar hypothesis was proposed by Haney et al (2022a, 2022b) to explain the dominant velocity increase northwest of the caldera measured with cross-station ambient noise correlations. We use Hypothesis-2 to explain the increase of seismic velocity at all stations across the island and provide reasoning for the spatial variations. In this hypothesis, the decrease of melt content still exists but is not the dominant factor causing the observed velocity increase.

Geological records suggest a northwestward migration of the active crater at Great Sitkin, with collapses of the northwestern flank (Waythomas et al., 2003b). The northwestern flank of the crater, with relatively young lava flows and sector collapses, is less consolidated and more susceptible to stress changes (e.g., dome weight and inflation/deflation) in comparison to other parts of the edifice (Haney et al., 2022a, 2022b; Waythomas et al., 2003b). This collapse scar results in more subsurface cracks on the northwestern side than on the southeastern side (Figure 3.4b). Consequently, with the co-eruptive magma extrusion and deflation, the closing of cracks has more effect on the weaker northwestern side, resulting

in a larger velocity increase as observed at GSSP (Figure 3.2; Haney et al., 2022a, 2022b). Additionally, tectonic faults may exist in the southeast quadrant (Ruppert et al., 2012), which may explain the observed shallow low-velocity zone below that area. Therefore, the increase in seismic velocity across the island is driven by the closing of cracks within shallow volcaniclastics with collapsed flanks and other faulting structures.

The findings in this study suggest the important role of eruptive magmatic processes in modifying the structure of the volcanic system. This structural modification may persist for an extended period. The exact duration of this magma extrusion-induced velocity increase is unclear, though it may last until the next eruption cycle with ceased lava effusion and increased magma recharge. A denser deployment of seismometers at Great Sitkin would provide higher-resolution data, enabling finer discrimination between the two hypotheses by capturing detailed spatial variations in seismic structure and velocity changes. This enhanced monitoring would offer insights into the specific location and extent of velocity changes, allowing for a more robust assessment of the dominant mechanisms driving the seismicity and velocity changes.

3.4 Conclusions for Great Sitkin Volcano

With single-station ambient noise interferometry, we observe changes in seismic velocities (dv/v) linked to eruptive behaviors. Our study proposes two hypotheses to explain seismic velocity changes during the eruptive period at Great Sitkin Volcano. Hypothesis-1 suggests the prominent velocity increase, notably at GSSP, is linked to processes near the magma reservoirs, aligning with a proposed double-reservoir system. The larger northwest reservoir induces a more significant velocity increase (2%-3%), supporting sustained magma supply. Hypothesis-2 offers an alternative explanation, emphasizing the closing of cracks within shallow volcanic sediments, especially on the weaker northwestern side which has experienced Holocene lava flows and flank collapses. Geological characteristics of this region contribute to a larger velocity increase during co-eruptive magma extrusion due to their higher susceptibility to pressure changes. Our findings emphasize the complexity of Great Sitkin's volcanic

system, with diverse co-eruptive structural modifications due to magma extrusion, resulting in seismic velocity variations.

4. SEISMIC VELOCITY CHANGES AT OKMOK VOLCANO

*Note: This chapter is a manuscript in preparation. The text has been reformatted to meet the thesis requirement. The data and methods section, as well as the supplementary materials, have been merged with Chapter 2 of this thesis. The manuscript is coauthored by Xiaotao Yang (Department of Earth, Atmospheric, and Planetary Sciences, Purdue University) and Jeremy Maurer (Department of Geosciences and Geological and Petroleum Engineering, Missouri University of Science and Technology).

Below is the citation information for this manuscript:

Kupres, C. A., Yang, X., & Maurer, J. (in preparation). Transient seismic velocity changes at Okmok Volcano reveal episodes of magma discharge and recharge.

4.1 Introduction

Okmok Volcano is located in northeastern Umnak Island within the Aleutian volcanic arc (Figure 4.1a; Miller et al., 1998). It erupted over 20 times during the past century, with the most recent explosive eruption on July 12, 2008 (Figure 4.1b). Previous studies have documented multiple phases of eruptive and non-eruptive seismic activity (Larsen et al., 2015; Ohlendorf et al., 2014) and surface deformation at Okmok (Freymueller and Kaufman, 2010; Masterlark et al., 2010; J. Wang et al., 2021; Xue et al., 2020) before and after the 2008 eruption, making it an ideal site to study the dynamics of magmatic systems at active volcanoes.

Okmok Volcano is a shield volcano with a broad basaltic profile, standing out among the volcanic landscapes of the Aleutian Islands (T. Miller et al., 1998). Its geological history is marked by a series of volcanic events that have shaped its current form. The construction of the pre-caldera volcano, followed by the formation of two overlapping calderas approximately 12,000 and 2050 years ago, highlights the complex and dynamic nature of Okmok's volcanic activity (Larsen et al., 2015; T. Miller et al., 1998). The presence of numerous parasitic cones, lava domes, and post-caldera features implies ongoing active volcanic processes within the region (T. Miller et al., 1998). Okmok's recent written history features one eruption in 1817 at Cone B, followed by every other eruption until 2008 being featured at Cone A (Larsen et al., 2015; Figure 4.1a). The 2008 eruption from July 12 to August 23 formed a new cone, named Ahmanilix, adjacent to Cone D within the caldera (Figure 4.1a). This explosive eruption produced ash plumes reaching remarkable heights, some towering over 16 km above

sea level. The eruption damaged infrastructure and caused flight cancellations across the North Pacific region (Larsen et al., 2015). The co-eruptive seismicity persisted until August 8, 2008, and gradually declined thereafter (Ohlendorf et al., 2014; Figure 4.1c).

The magmatic system beneath Okmok Volcano showcases a complex network of reservoirs and conduits (Bennington et al., 2018; Kasatkina et al., 2022; Masterlark et al., 2010; Ohlendorf et al., 2014; J. Wang et al., 2021; Xue et al., 2020). At depths below 10 km, a primary magma conduit is identified, serving as a crucial pathway for magma ascent and volcanic evolution (Kasatkina et al., 2022; Masterlark et al., 2010; Ohlendorf et al., 2014). This conduit is associated with a significantly high Vp/Vs ratio, potentially indicative of its long-term activity and contribution to the volcano's formation (Kasatkina et al., 2022). Above it lies a substantial magma reservoir, connected to several shallow low-velocity anomalies beneath the caldera's inner perimeter. Notably, one of the shallow anomalies is below Cone A, interpreted as a primary source for historical eruptions (Kasatkina et al., 2022).

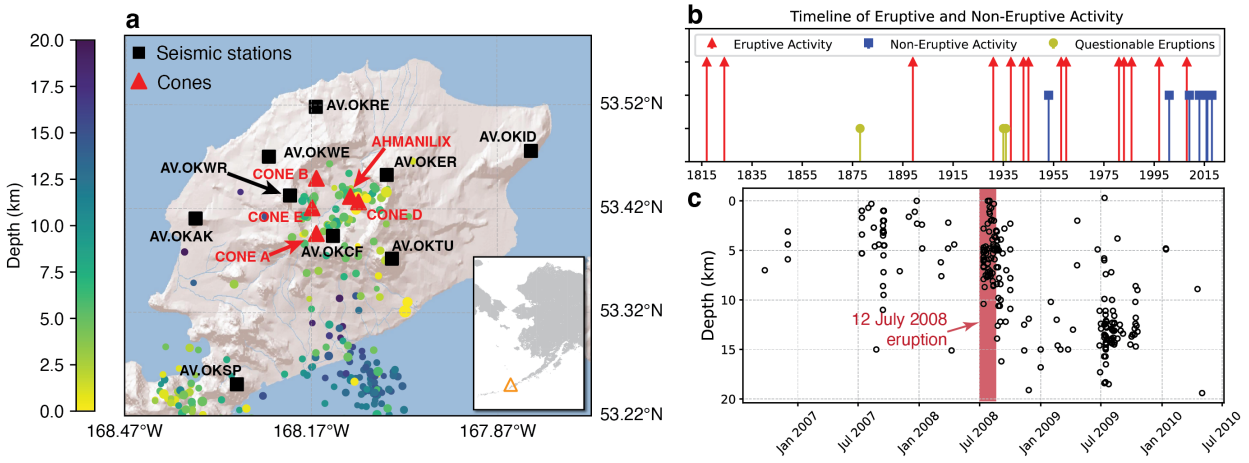

Figure 4.1. Seismic stations with volcanic features and activity on Umnak Island centering on Okmok Volcano. (a) Distribution of seismic stations (black squares), volcanic cones (red triangles), and earthquakes (magnitude $\geq$1) from July 2006 to July 2010 from USGS Comprehensive Earthquake Catalog (ComCat) (U.S. Geological Survey, 2022) (dots color-coded by depths and scaled by magnitudes). (b) Past activity of Okmok since 1817 from Alaska Volcano Observatory, including eruptive activity, non-eruptive activity, and questionable eruptions. (c) Distribution of earthquake depths with time for the same catalog as (a).

Additionally, Kasatkina et al. (2022) proposed a shallow ductile layer at depths of 2-5 km, acting as a barrier for vertical magma ascent, except in rare instances. Overall, the configuration of the magmatic system beneath Okmok reflects a dynamic interplay of geological processes, influencing its eruptive behavior and long-term evolution. Despite previous studies, the mechanism driving the seismicity and deformation at Okmok Volcano, as well as the interactions between the magmatic system and the surrounding geological structures, is unclear. Addressing these gaps is crucial for accurately assessing volcanic hazards and improving our ability to forecast eruptions.

To understand the underlying structural modifications and mechanical processes associated with the 2008 explosive eruption, we measure changes in seismic velocity (dv/v) over four years from July 2006 to July 2010, approximately centering on the 2008 eruption. By covering the pre-, co-, and post eruptive time frames, we examine the temporal and spatial variations in seismic velocity changes likely associated with the magmatic processes beneath Okmok. To facilitate the interpretation, we compare the velocity changes with earthquake activity and surface deformation from InSAR data analyses. This integrated approach contributes to understanding volcanic unrest and eruption precursors, ultimately enhancing volcanic hazard assessment and monitoring efforts.

4.2 Results

We compare the dv/v results with the seismicity history from the USGS Comprehensive Catalog (U.S. Geological Survey, 2022) and the InSAR deformation series (Figure 4.2c). We show the spatial distribution of the dv/v at six selected dates in Figure 4.4. In the following paragraphs, we describe major dv/v features and the corresponding seismicity and surface deformation patterns. Our description of major dv/v patterns is based primarily on the 1-2 Hz estimates, with the 0.4-1 Hz results for comparison.

4.2.1 Major *dv/v* features

Pre-eruptive dv/v variations are relatively subtle, varying among different frequencies. Before the July 12, 2008, eruption, the dv/v results at 1-2 Hz display minor variations

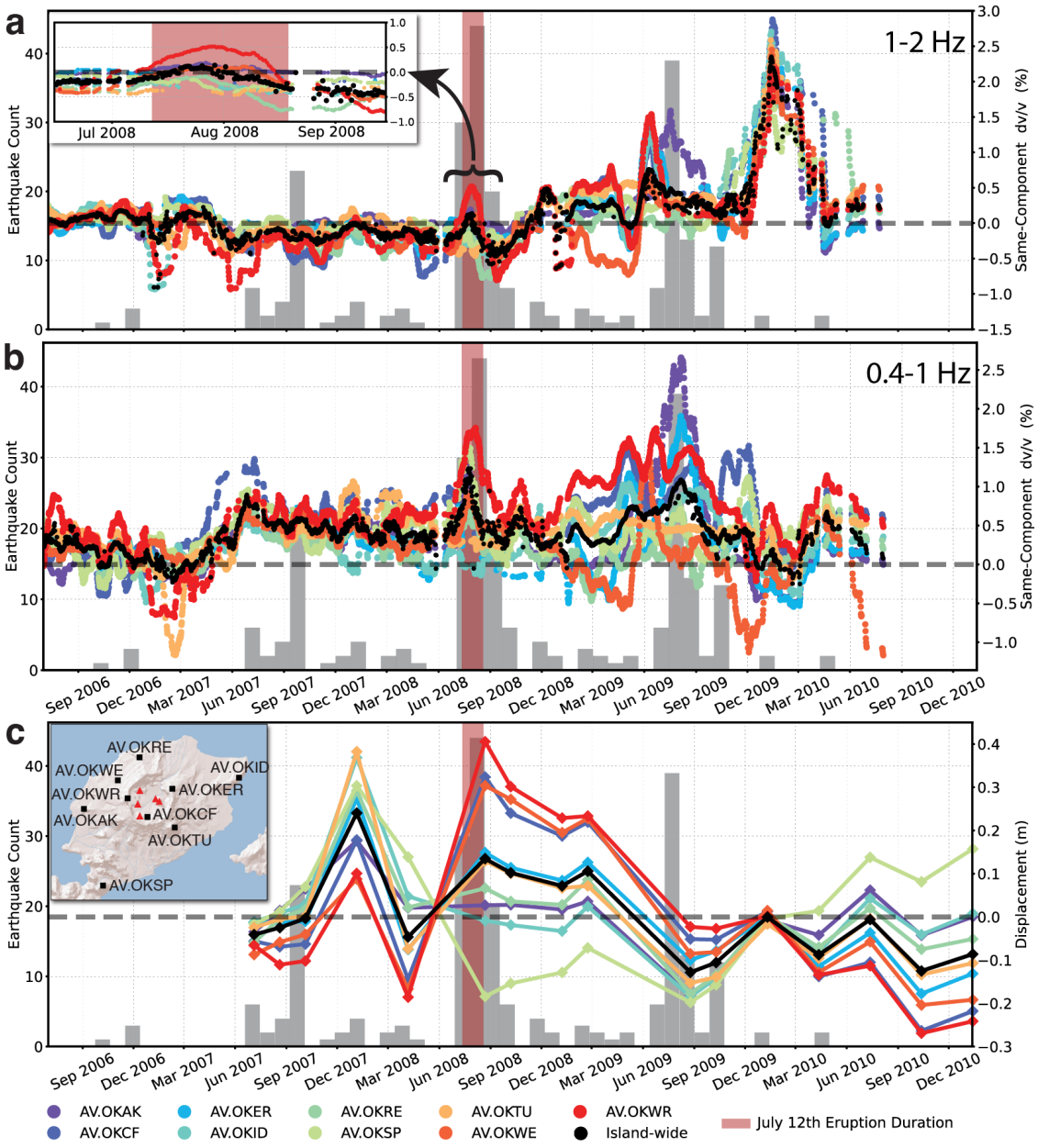

Figure 4.2. Changes in seismic velocity from Z-component autocorrelation and ground deformation from InSAR analysis. Data was smoothed using a 20-day moving window mean for all plots. (a-b) *dv/v* results at 1-2 Hz (a) and 0.4-1 Hz (b) from July 2006 to July 2010 at all stations color-coded as in (c). The grey histogram shows the earthquake count around Okmok Volcano with the same catalog as for Figure 4.1a. An average *dv/v* is shown in black. (c) InSAR ground deformation series from July 2007 to April 2010 extracted at corresponding seismic stations as in (a-b).

(-0.5% to 0.5%), with a long-term (about 1.5 years) decreasing trend. One exception is the *dv/v* results between December 2006 and July 2007, when some stations experienced abrupt decreases (Figure 4.2a). However, this decrease in velocity does not correlate with any notable seismicity changes. In comparison, the *dv/v* results at 0.4-1 Hz show stronger variations (-1% to 1%) before the 2008 eruption than those at 1-2 Hz with different overall patterns (Figure 4.2b). Specifically, there is a slight decreasing trend from July 2006 to March 2007, followed by an increase until June 2007 to about 0.5%. This minor spike in *dv/v* precedes a peak in seismicity (Figure 4.2b) above about 10 km (Figure 4.1c). A subtle decrease continued until the eruption on July 12, 2008.

During the co-eruptive phase from July to August 2008, there is an increase in seismic velocity, followed by a pronounced decrease. This behavior precedes a subsequent rise since September 2008, ultimately maintaining an elevated level until April 2009.

We observed two post-eruptive *dv/v* spikes during our observation period. The first spike occurred between July 2009 and October 2009, preceding an increase in seismic activity (Figure 4.2a and 4.3). On average across all stations (Figure 4.3), the *dv/v* in the 1-2 Hz band decreased from approximately 0.25% to 0%, followed by a rise to about 0.75% in *dv/v*. This spike reverted to about 0.25% in July 2009, coinciding with a localized escalation in seismic activity that ended in October 2009. Notably, station AV.OKAK portrayed a similar *dv/v* pattern but with a delay of about 1.5 months (purple dots in Figure 4.2), returning to its pre-spike level in October 2009. The second post-eruptive spike occurred as a large increase in *dv/v* from January 2010 to April 2010. This occurred during a non-eruptive phase and a seismically quiet period and was consistently observed across all stations. The velocity change reached up to about 3% at station AV.OKCF in the southern caldera (Figure 4.2a). The average peak amplitude across all stations was about 2-2.5% (Figure 4.2a and 4.3).

In comparison, the 0.4-1 Hz *dv/v* results show an opposite relationship in terms of the relative amplitudes of the two post-eruptive spikes (Figure 4.2b). Specifically, the amplitudes coinciding with the first post-eruptive spike in the middle of 2009 are larger than the second spike in early 2010. The average *dv/v* for the first spike is about 1%, with some stations up to 2.5%. The average amplitude for the second spike is about 0.75%, with localized spikes

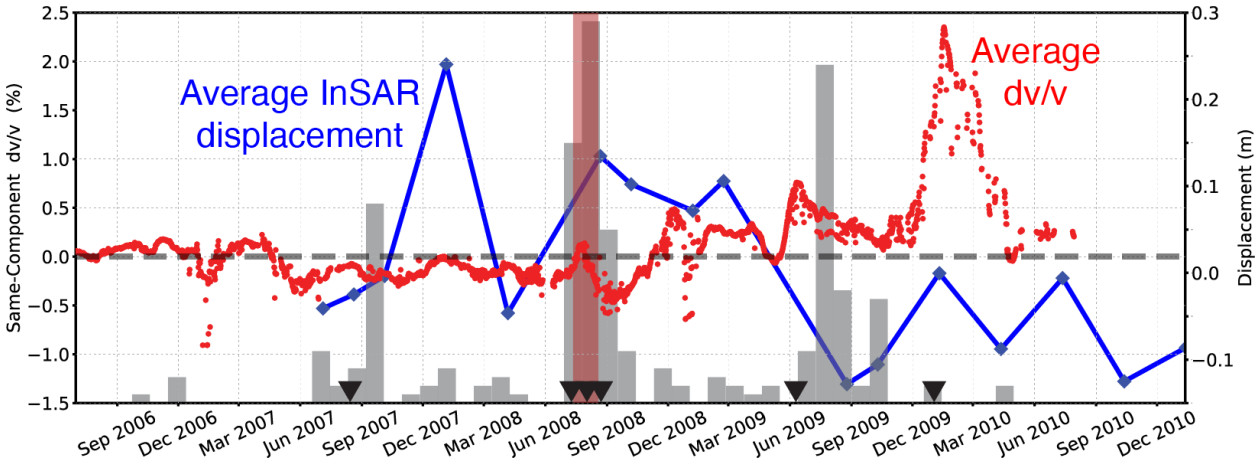

Figure 4.3. Comparison of the average 1-2 Hz *dv/v* results (red) and ground deformation estimates (blue). The grey histogram shows the earthquake count around Okmok Volcano with the same catalog as in Figure 4.1a. The inverted black triangles at the bottom mark selected dates for the spatial distribution of *dv/v* in Figure 4.4.

up to 1.25%. Nonetheless, the existence and times of these two post-eruptive spikes are consistent across the two frequency bands.

The spatial distribution of the *dv/v* on selected dates reveals a possible increased sensitivity to *dv/v* changes within the caldera and on its rim (Figure 4.4). During *dv/v* spikes, there is a slightly more pronounced effect within the caldera. This is most prominent during the co-eruptive spike in which the AV.OKWR station at the southwestern caldera rim exhibits the largest increase (Figures 4.2a and 4.4c). However, there is no notable spatial pattern during other *dv/v* spikes.

4.2.2 Ground movement from InSAR time series

During the pre-eruption and co-eruptive phases (April 2008 to the end of the eruption in August 2008), we observe a variable range of inflation and deflation across the station locations (Figure 4.2c). However, due to the limited temporal coverage of ALOSs dataset over Okmok, the temporal resolution of the co-eruptive ground movement is low.

Following the eruption, we observe a distinct shift, marked by post-eruption deflation that persisted until August 2009. During this period, all stations display a consistent trend of deflation. However, a pause in deflation is observed across all stations from August 2009 until January 2010, introducing a temporary deviation in the displacement pattern. The lack of temporal resolution makes it impossible to determine the exact date the deflation paused. However, this deviation coincides with the spike in dv/v and seismicity in June-July 2009. Since then, the examined sites have shown fluctuations that continued at least to the end of the dataset. The island-wide average ground movement history indicates an overall deflation trend since early 2008 (Figure 4.3).

4.3 Discussion

The observed dv/v results reveal several notable spikes, including a minor co-eruptive increase in July to August 2008 and two subsequent island-wide spikes in June to July 2009 and December 2009 to March 2010. These spikes represent distinct phases of volcanic activity involving magma extrusion and recharge (Figure 4.5). The co-eruptive event may indicate deflation and closing of cracks with reservoir depressurization as the result of magma extrusion. The post-eruptive dv/v spikes coincide with periods of non-eruptive surface displacement fluctuations, reflecting magma recharge events. The temporal distribution and characteristics of these peak velocity increases provide valuable insights into the dynamics of volcanic processes, which we discuss in detail in the following paragraphs.

4.3.1 Co-eruptive dv/v increase due to magma withdrawal

At Okmok, we observe a co-eruptive increase that is likely the consequence of magma extrusion and loading of the new volcaniclastic deposits. The dv/v spike shows a similar characteristic to the observation during the 2004 eruption at Veniaminof Volcano (Bennington et al., 2018), which is attributed to the consequence of the depressurization of the magma storage system and the sealing of fractures with the extrusion of magmatic fluids. At Okmok, we also observe co-eruptive deflations across the island (Figure 4.2c). Following the onset of the 2008 eruption, the extraction of magma from the reservoir would lead to a drop in

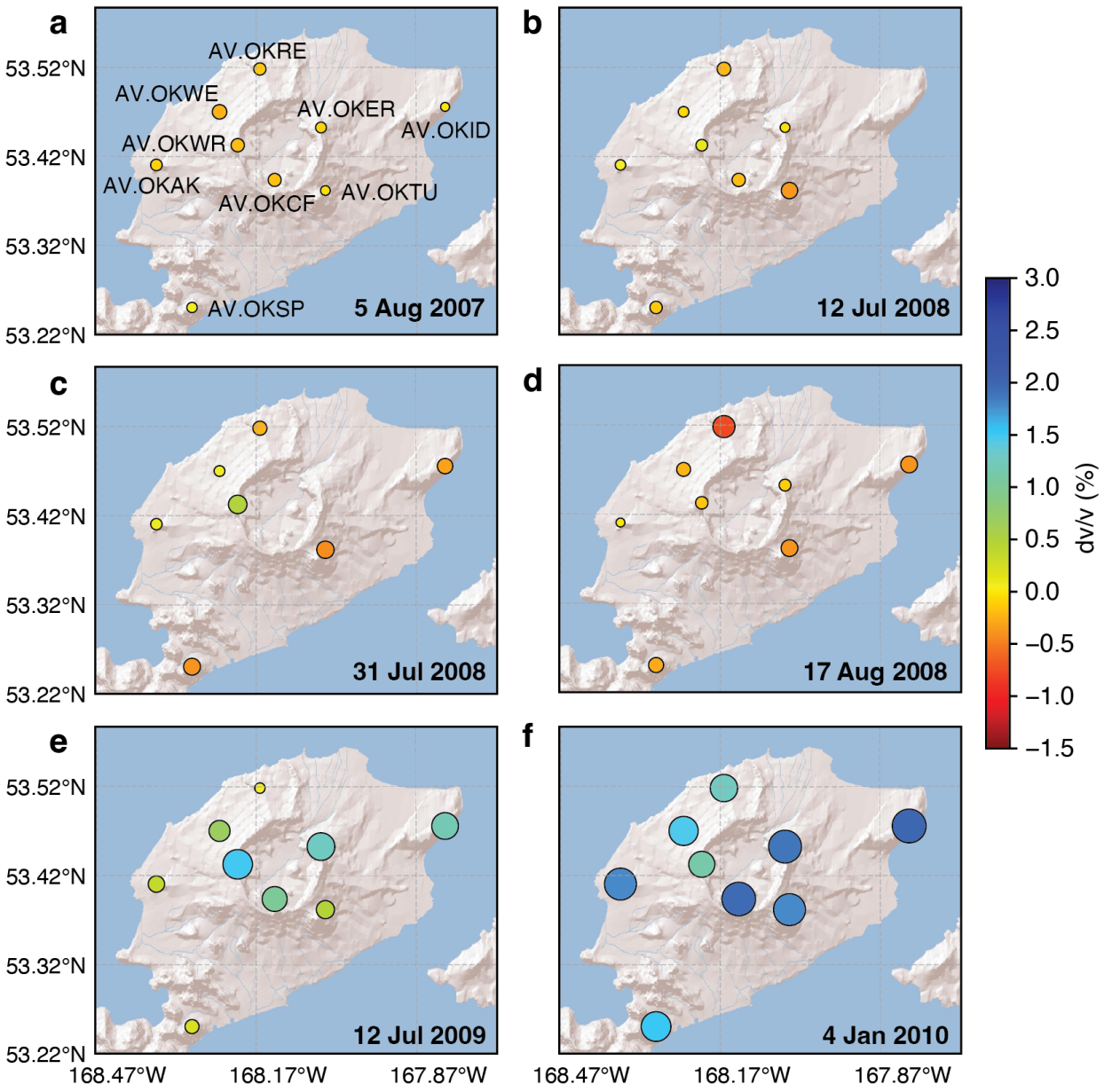

Figure 4.4. Spatial distribution of the dv/v results at selected dates measured at 1-2 Hz. The circle at each station is scaled by their absolute dv/v value and color-corded by the true amplitude. Station names are labeled in (a) for reference. The dates are marked in Figure 4.3 (black triangles at the bottom).

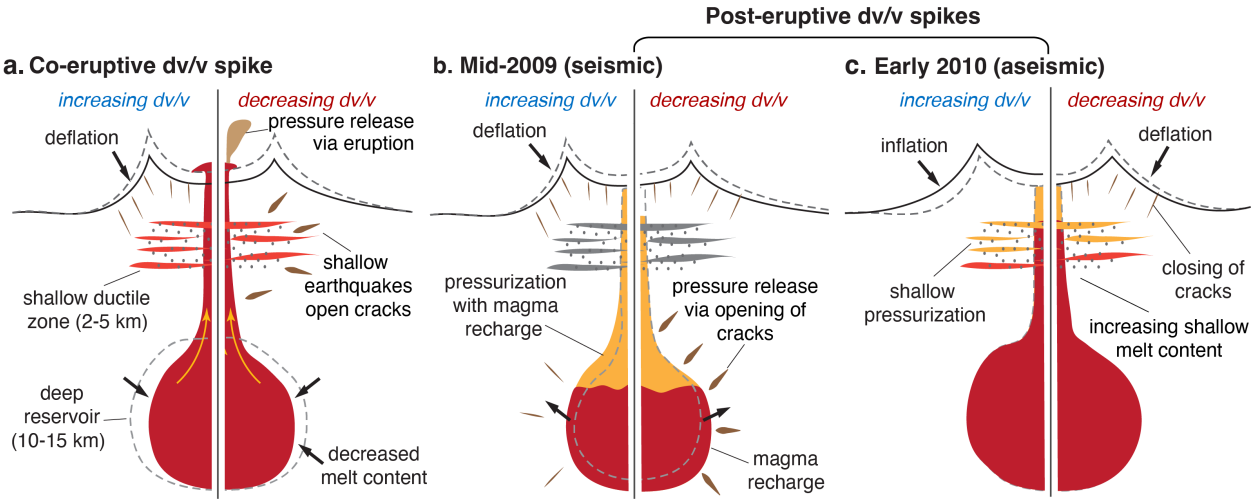

Figure 4.5. Diagrams illustrating the magmatic processes associated with the observed seismic velocity changes. (a) Co-eruptive *dv/v* increase as the result of magma extrusion, with deflation at the surface, followed by a decrease due to depressurization and the occurrence of earthquakes. (b) Mid-2009 *dv/v* increase as the response to pressurization due to recharge of the deep magma reservoir, followed by a decrease with earthquakes and pressure release via inflation. (c) An increase in *dv/v* responding to shallow magma recharge with pressurization in the ductile zone, followed by a decrease in *dv/v* due to inflation and depressurization. The split views on the left and right halves show drivers for the increase and decrease phases, respectively. Diagrams are not to scale.

pressure and may induce deflation of the volcano (Peltier et al., 2010). This process would be accompanied by the sealing of fractures in the surrounding medium (Duputel et al., 2009; Rivet et al., 2014; Sens-Schönfelder et al., 2014) and the decrease of pore spaces beneath the volcano (Figure 4.5a). These processes, as the consequences of magma extrusion, would prompt an increase in seismic velocities. Additionally, the emplacement of the new tephra cone, Ahmanilix (Larsen et al., 2015), is a notable product of the eruption. The lithostatic loading from this new cone, similar to snow and glaciers (Donaldson et al., 2019; Mordret et al., 2016), could also contribute to the increase in shallow subsurface seismic velocity at nearby stations (Q.-Y. Wang et al., 2017).

During the co-eruptive *dv/v* spikes, seismic activity reached its peak with earthquakes up to a magnitude of 3.5 (U.S. Geological Survey, 2022). Earthquake damages would reduce the

seismic velocity due to damage and potentially lead to the opening of cracks and the increase of permeability (Lesage et al., 2014; Wegler et al., 2009). Therefore, the heightened seismicity may have helped maintain the velocity increase at a relatively low level by canceling part of the velocity increase due to deflation and the reduction of melt content. However, they are likely the dominant contributor to the subsequent decrease in the *dv/v* (Figure 4.5a). The velocity decrease is the result of alterations in subsurface conditions caused by the intense co-eruptive seismic activity.

4.3.2 Post-eruptive *dv/v* spikes due to magma recharge

The island-wide *dv/v* spike in the middle of 2009 reflects an intense magma recharge event that eventually caused a swarm of earthquakes (Figure 4.2a). Concurrently, the volcano is nearing the end of a deflation phase (Figure 4.2c), a characteristic of post-eruption subsidence (Dzurisin et al., 2019; McGimsey et al., 2014; J. Wang et al., 2021). Spatially, the *dv/v* spike shows minimal variation at the increasing stage. During the relaxation phase, AV.OKAK takes 3 months longer to return to the baseline level than the other stations.

We argue that the mid-2009 spike in *dv/v* and the subsequent surface inflection are caused by the onset of an episode of relatively deep magma recharge (Figure 4.5b). The depth of the earthquakes (>10 km) seen in the south part of the study area (Figure 4.1a and c) aligns with the magma conduit system below 10 km inferred by Kasatkina et al. (2022). While this zone of seismicity is outside their model resolution, they imaged horizontally elongated low-velocity anomalies that may connect this zone with the caldera. Furthermore, the *dv/v* at 0.4-1 Hz (Figure 4.2b) shows larger amplitudes of the first post-eruptive spike than the second one, whereas the 1-2 *dv/v* at Hz (Figure 4.2b) demonstrates an opposite relationship. Considering that lower frequencies are more sensitive to larger volumes Yuan et al., 2021, the larger amplitudes of the 0.4-1 Hz indicate that the first post-eruptive spike may be sourced deeper with a larger spatial extent than the second one. The resultant increase in pressure due to magma recharge seals the cracks within the subsurface. This process leads to an increase in *dv/v*, similar to that documented by Donaldson et al. (2017) at Kilauea Volcano in Hawaii. The subsequent decrease in *dv/v* is the result of pressure release via re-opening

of the cracks (Carrier et al., 2015), followed by a surge in earthquake activity (Scuderi et al., 2016) (Figure 4.2a-b). Although the temporal resolution of the InSAR data is limited, the temporal proximity to the inferred recharge indicates that the change from deflation to inflation, after the dv/v spike and seismicity swarm, is a consequence due to the onset of the magma recharge event.

The second post-eruptive dv/v spike from December 2009 to May 2010 across the island suggests a second phase of relatively slow and aseismic magma recharge (Figure 4.5c). This spike coincides with minimal seismic activity and the first post-eruptive oscillation of surface displacement around the volcano (Figures 4.2a and c). Bennington et al. (2015) note the recurrent cycles of inflation and deflation since the 2008 eruption at Okmok since January 2013, the beginning of their observation period. They propose that these rapid, small amplitudes, aseismic inflationary events suggest the recharge of the shallow magma reservoir directly beneath the caldera as shown in seismic tomographic images (Masterlark et al., 2010; Ohlendorf et al., 2014). These observations resemble the coincidence of the surface deformation pattern with the dv/v spike in early 2010. The seismic velocity increase serves as an indicator of recharge in the shallow magma reservoir (Figure 4.5c). The period encompassing this dv/v spike is nearly completely aseismic, with only four earthquakes ranging in magnitudes from 1.7 to 2.7 in the USGS ComCat catalog (U.S. Geological Survey, 2022). These earthquakes would not significantly affect the seismic velocity. The duration of this magma recharge event, as indicated by the period of increase in dv/v, is about 5-6 months. Compared to the mid-2009 magma recharge, this phase of magma recharge is much slower and less intense. The relatively slow recharge might have prevented earthquakes, at least in the detectable magnitudes.

4.4 Conclusions for Okmok Volcano

Utilizing single-station ambient noise interferometry, we delineate transient seismic velocity changes associated with eruptive activities at Okmok Volcano. The dv/v results show three distinct spikes relating to magmatic activity, including one co-eruptive spike and two post-eruptive spikes. The co-eruptive dv/v increase in July to August 2008 reflects the con-

sequence of magma extrusion and loading of volcanic sediments, leading to reservoir depressurization and sealing of fractures. This increase was accompanied by co-eruptive deflation and increased seismic activity, the latter of which would led to the reduction of the seismic velocity. Subsequent post-eruptive *dv/v* spikes in mid-2009 and early 2010 suggest two major episodes of magma recharge. The mid-2009 spike increase was the result of subsurface pressurization and crack sealing due to deflation. The subsequent decrease was due to the damage of crustal materials corresponding to the increased seismicity at depths near the deep reservoir. The early 2010 spike was also a recharge event but was less intense and aseismic. The increase was due to magma recharge reaching the shallow magma reservoir leading to the increase in pressure. This was followed by inflation at some stations, together with the increase in melt content, leading to the subsequent velocity decrease. The spatial and temporal variations in *dv/v* provide insights into the depth and intensity of magmatic processes. The integration of *dv/v* monitoring with seismicity and surface deformation enhances our understanding of volcanic unrest and eruption precursors, contributing to improved volcanic hazard assessment.

5. CONCLUSION

Utilizing single-station seismic velocity, the findings in this thesis at Great Sitkin and Okmok Volcanoes reveal significant insights into the relationships between seismic velocity changes and eruptive behaviors. At Great Sitkin, two hypotheses were proposed to delineate the observed seismic velocity variations during eruptive periods. Hypothesis-1 suggests that the notable velocity increase at GSSP is attributed to processes near the northwest magma reservoir, supporting a double-reservoir system. The larger northwestern reservoir is close to a substantial velocity increase, supporting its role in a sustained magma supply. Hypothesis-2 emphasizes the closure of cracks within shallow volcanic sediments, particularly on the weaker northwestern side, leading to a larger velocity increase during co-eruptive magma extrusion. These findings provided insight into the complexity of Great Sitkin's volcanic system, revealing diverse structural modifications during eruptive phases.

At Okmok Volcano, the transient seismic velocity changes delineate the distinct phases of eruptive activity. Three notable dv/v spikes are observed, indicating magmatic processes. The co-eruptive spike in July to August 2008 reflects magma extrusion and volcanic sediment loading, leading to reservoir depressurization and fracture sealing. Subsequent post-eruptive spikes in mid-2009 and early 2010 suggest major episodes of magma recharge. In mid-2009, increased pressure and crack sealing from deflation caused a spike. Later, crustal damage led to a decrease linked to heightened seismicity. Early 2010 saw an aseismic spike that was attributed to magma recharge and increasing pressure in the shallow reservoir. This led to inflation and increased melt content subsequently decreasing velocity. The integration of dv/v monitoring with seismicity and surface deformation improves our understanding of volcanic unrest, contributing to improved volcanic hazard assessment.

The research reported in this thesis showcased the utility of computing single-station changes in seismic velocity for understanding volcanic systems. However, the research project also demonstrated the need for complementary datasets. For example, velocity models and deformation data helped to gain a more comprehensive view of subsurface structural modification when considered in conjunction with dv/v. Seismic velocity monitoring remains a new field for volcanic monitoring. Studying different and diverse volcanic settings, such as

Great Sitkin and Okmok, contributed to gaining insights into magma dynamics, reservoir processes, and structural modifications. This would ultimately improve our ability to assess volcanic hazards and forecast eruptions at volcanoes globally.

REFERENCES

Alaska Volcano Observatory. (2021a, May). *Volcano Observatory Notice for Aviation* (tech. rep.). U.S. Geological Survey, Alaska Volcano Observatory. Anchorage, AK.

Alaska Volcano Observatory. (2021b, July). *Volcano Observatory Notice for Aviation* (tech. rep.). U.S. Geological Survey, Alaska Volcano Observatory. Anchorage, AK.

Alaska Volcano Observatory/USGS. (1988). *Alaska Volcano Observatory* (tech. rep.). International Federation of Digital Seismograph Networks. Anchorage, AK. https://doi.org/10.7914/SN/AV

Bennington, N., Haney, M., Thurber, C., & Zeng, X. (2018). Inferring magma dynamics at Veniaminof Volcano via application of ambient noise. *Geophysical Research Letters*, *45*(21), 11, 650–11, 658. https://doi.org/10.1029/2018GL079909

Bishop, J. W., Haney, M. M., Fee, D., Matoza, R. S., McKee, K. F., & Lyons, J. J. (2023). Backazimuth estimation of airtoground coupled infrasound from transverse coherence minimization. *The Seismic Record*, *3*(4), 249–258. https://doi.org/10.1785/0320230023

Brenguier, F., Shapiro, N. M., Campillo, M., Ferrazzini, V., Duputel, Z., Coutant, O., & Nercessian, A. (2008). Towards forecasting volcanic eruptions using seismic noise. *Nature Geoscience*, *1*(2), 126–130. https://doi.org/10.1038/ngeo104

Brown, S. K., Loughlin, S. C., Sparks, R., Vye-Brown, C., Barclay, J., Calder, E., Cottrell, E., Jolly, G., Komorowski, J.-C., Mandeville, C., Newhall, C., Palma, J., Potter, S., & Valentine, G. (2015, July). Global volcanic hazard and risk. In S. C. Loughlin, R. Sparks, S. K. Brown, S. Jenkins, & C. Vye-Brown (Eds.). Cambridge University Press. https://doi.org/10.1017/CBO9781316276273.004

Carrier, A., Got, J.-L., Peltier, A., Ferrazzini, V., Staudacher, T., Kowalski, P., & Boissier, P. (2015). A damage model for volcanic edifices: Implications for edifice strength, magma pressure, and eruptive processes. *Journal of Geophysical Research: Solid Earth*, *120*(1), 567–583. https://doi.org/10.1002/2014JB011485

Chen, C., & Zebker, H. (2002). Phase unwrapping for large SAR interferograms: Statistical segmentation and generalized network models. *IEEE Transactions on Geoscience and Remote Sensing*, *40*(8), 1709–1719. https://doi.org/10.1109/TGRS.2002.802453

Chen, C., & Zebker, H. A. (2001). Two-dimensional phase unwrapping with use of statistical models for cost functions in nonlinear optimization. *JOSA A*, *18*(2), 338–351. https://doi.org/10.1364/JOSAA.18.000338

Cubuk-Sabuncu, Y., Jónsdóttir, K., Caudron, C., Lecocq, T., Parks, M. M., Geirsson, H., & Mordret, A. (2021). Temporal seismic velocity changes during the 2020 rapid inflation at Mt. Þorbjörn-Svartsengi, Iceland, using seismic ambient noise. *Geophysical Research Letters*, *48*(11), e2020GL092265. https://doi.org/10.1029/2020GL092265

De Plaen, R. S. M., Lecocq, T., Caudron, C., Ferrazzini, V., & Francis, O. (2016). Single-station monitoring of volcanoes using seismic ambient noise. *Geophysical Research Letters*, *43*(16), 8511–8518. https://doi.org/10.1002/2016GL070078

Delph, J. R., Ward, K. M., Zandt, G., Ducea, M. N., & Beck, S. L. (2017). Imaging a magma plumbing system from MASH zone to magma reservoir. *Earth and Planetary Science Letters*, *457*, 313–324. https://doi.org/10.1016/j.epsl.2016.10.008

Dietterich, H., Plank, S., & Loewen, M. (2023, January). *Multi-sensor remote sensing of effusive eruption dynamics and lava flow morphology at Great Sitkin Volcano, Alaska*. IAVCEI.

Donaldson, C., Winder, T., Caudron, C., & White, R. S. (2019). Crustal seismic velocity responds to a magmatic intrusion and seasonal loading in Icelands northern volcanic zone. *Science Advances*, *5*(11), eaax6642. https://doi.org/10.1126/sciadv.aax6642

Duputel, Z., Ferrazzini, V., Brenguier, F., Shapiro, N., Campillo, M., & Nercessian, A. (2009). Real time monitoring of relative velocity changes using ambient seismic noise at the Piton de la Fournaise volcano (La Réunion) from January 2006 to June 2007. *Journal of Volcanology and Geothermal Research*, *184*(12), 164–173. https://doi.org/10.1016/j.jvolgeores.2008.11.024

Dzurisin, D., Lu, Z., Poland, M. P., & Wicks, C. W. J. (2019). Space-based imaging radar studies of U.S. volcanoes. *Frontiers in Earth Science*, *6*. https://doi.org/10.3389/feart.2018.00249

Farr, T. G., Rosen, P. A., Caro, E., Crippen, R., Duren, R., Hensley, S., Kobrick, M., Paller, M., Rodriguez, E., Roth, L., Seal, D., Shaffer, S., Shimada, J., Umland, J., Werner, M., Oskin, M., Burbank, D., & Alsdorf, D. (2007). The shuttle radar topography mission. *Reviews of Geophysics*, *45*(2). https://doi.org/10.1029/2005RG000183

Feng, K.-F., Huang, H.-H., & Wu, Y.-M. (2020). Detecting pre-eruptive magmatic processes of the 2018 eruption at Kilauea, Hawaii volcano with ambient noise interferometry. *Earth, Planets and Space*, *72*(1), 74. https://doi.org/10.1186/s40623-020-01199-x

Freymueller, J. T., & Kaufman, A. M. (2010). Changes in the magma system during the 2008 eruption of Okmok Volcano, Alaska, based on GPS measurements. *Journal of Geophysical Research: Solid Earth*, *115*. https://doi.org/10.1029/2010JB007716

Global Volcanism Program. (2021, September). *Report on Great Sitkin (United States) (Sennert, S, ed.). Weekly Volcanic Activity Report, 8 September-14 September 2021* (tech. rep.). Smithsonian Institution and US Geological Survey. Washington D.C., USA.

Global Volcanism Program. (2023, March). *Report on Great Sitkin (United States) (Sennert, S, ed.). Weekly Volcanic Activity Report, 22 March-28 March 2023* (tech. rep.). Smithsonian Institution and US Geological Survey. Washington D.C., USA.

Haney, M. M., Miller, D. J., Hotovec-Ellis, A. J., Thurber, C. H., & Dietterich, H. R. (2022a). Time-lapse seismic velocity changes coincident with dome emplacement at Great Sitkin Volcano, Alaska. *SSA Annual Meeting*, *93*, Number 2B.

Haney, M. M., Miller, D. J., Hotovec-Ellis, A. J., Thurber, C. H., Dietterich, H. R., & Yang, X. (2022b). Time-lapse seismic velocity changes coincident with dome emplacement at Great Sitkin Volcano, Alaska. *AGU Fall Meeting*, *2022*, V33A–03. https://ui.adsabs.harvard.edu/abs/2022AGUFM.V33A..03H/abstract

Kasatkina, E., Koulakov, I., Grapenthin, R., Izbekov, P., Larsen, J. F., Al Arifi, N., & Qaysi, S. I. (2022). Multiple magma sources beneath the Okmok caldera as inferred from local earthquake tomography. *Journal of Geophysical Research: Solid Earth*, *127*(10), e2022JB024656. https://doi.org/10.1029/2022JB024656

Larsen, J. F., Neal, C. A., Schaefer, J. R., Kaufman, A. M., & Lu, Z. (2015). The 2008 phreatomagmatic eruption of Okmok Volcano, Aleutian Islands, Alaska: Chronology, deposits, and landform changes. *Alaska Division of Geological & Geophysical Surveys Report of Investigation*, RI 2015–2. https://doi.org/10.14509/29405

Lees, J. M. (2007). Seismic tomography of magmatic systems. *Journal of Volcanology and Geothermal Research*, *167*(14), 37–56. https://doi.org/10.1016/j.jvolgeores.2007.06.008

Lesage, P., Reyes-Dávila, G., & Arámbula-Mendoza, R. (2014). Large tectonic earthquakes induce sharp temporary decreases in seismic velocity in Volcán de Colima, Mexico. *Journal of Geophysical Research: Solid Earth*, *119*(5), 4360–4376. https://doi.org/10.1002/2013JB010884

Luo, B., Zhang, S., & Zhu, H. (2023). Monitoring seasonal fluctuation and long-term trends for the Greenland ice sheet using seismic noise auto-correlations. *Geophysical Research Letters*, *50*(7), e2022GL102146. https://doi.org/10.1029/2022GL102146

Masterlark, T., Haney, M., Dickinson, H., Fournier, T., & Searcy, C. (2010). Rheologic and structural controls on the deformation of Okmok Volcano, Alaska: Fems, insar, and ambient noise tomography. *Journal of Geophysical Research: Solid Earth*, *115*(B2). https://doi.org/10.1029/2009JB006324

McGimsey, R. G., Neal, C. A., Girina, O. A., Chibisova, M., & Rybin, A. (2014). *2009 volcanic activity in Alaska, Kamchatka, and the Kurile Islands: Summary of events and response of the Alaska Volcano Observatory*. https://doi.org/10.3133/sir20135213

Miller, D., Bennington, N., Haney, M., Bedrosian, P., Key, K., Thurber, C., Hart, L., & Ohlendorf, S. (2020). Linking magma storage and ascent to eruption volume and composition at an arc caldera. *Geophysical Research Letters*, *47*(14), e2020GL088122. https://doi.org/10.1029/2020GL088122

Miller, T., McGimsey, R. G., Richter, D. H., Riehle, J. R., Nye, C., Yount, M. E., & Dumoulin, J. A. (1998). Catalog of the historically active volcanoes of Alaska. *U.S. Geological Survey Open-File Report*. https://doi.org/10.3133/OFR98582

Mordret, A., Mikesell, T. D., Harig, C., Lipovsky, B. P., & Prieto, G. A. (2016). Monitoring southwest Greenlands ice sheet melt with ambient seismic noise. *Science Advances*, *2*(5), e1501538. https://doi.org/10.1126/sciadv.1501538

National Academies of Sciences, E., & Medicine. (2017, July). *Volcanic eruptions and their repose, unrest, precursors, and timing*. National Academies Press. https://doi.org/10.17226/24650

Ohlendorf, S. J., Thurber, C. H., Pesicek, J. D., & Prejean, S. G. (2014). Seismicity and seismic structure at Okmok Volcano, Alaska. *Journal of Volcanology and Geothermal Research*, *278279*, 103–119. https://doi.org/10.1016/j.jvolgeores.2014.04.002

Olivier, G., Brenguier, F., Carey, R., Okubo, P., & Donaldson, C. (2019). Decrease in seismic velocity observed prior to the 2018 eruption of Klauea Volcano with ambient seismic noise interferometry. *Geophysical Research Letters*, *46*(7), 3734–3744. https://doi.org/10.1029/2018GL081609

Orr, T. R., Dietterich, H. R., Fee, D., Girona, T., Grapenthin, R., Haney, M. M., Loewen, M. W., Lyons, J. J., Power, J. A., Schwaiger, H. F., Schneider, D. J., Tan, D., Toney, L., Wasser, V. K., & Waythomas, C. F. (2024). *2021 volcanic activity in Alaska and the Commonwealth of the Northern Mariana Islandssummary of events and response of the Alaska Volcano Observatory*. https://doi.org/10.3133/sir20245014

Paulatto, M., Hooft, E. E. E., Chrapkiewicz, K., Heath, B., Toomey, D. R., & Morgan, J. V. (2022). Advances in seismic imaging of magma and crystal mush. *Frontiers in Earth Science*, *10*. https://doi.org/https://doi.org/10.3389/feart.2022.970131

Peltier, A., Staudacher, T., & Bachèlery, P. (2010). New behaviour of the Piton de La Fournaise volcano feeding system (La Réunion Island) deduced from GPS data: Influence of the 2007 Dolomieu caldera collapse. *Journal of Volcanology and Geothermal Research*, *192*(12), 48–56. https://doi.org/10.1016/j.jvolgeores.2010.02.007

Pesicek, J. D., Thurber, C. H., DeShon, H. R., Prejean, S. G., & Zhang, H. (2008). Three-dimensional P-wave velocity structure and precise earthquake relocation at Great Sitkin Volcano, Alaska. *Bulletin of the Seismological Society of America*, *98*, 2428–2448. https://doi.org/10.1785/0120070213

Power, J., Stihler, S., White, R., & Moran, S. (2004). Observations of deep long-period (DLP) seismic events beneath Aleutian arc volcanoes; 19892002. *Journal of Volcanology and Geothermal Research*, *138*, 243–266. https://doi.org/10.1016/j.jvolgeores.2004.07.005

Rivet, D., Brenguier, F., Clarke, D., Shapiro, N. M., & Peltier, A. (2014). Long-term dynamics of Piton de la Fournaise volcano from 13 years of seismic velocity change measurements and GPS observations. *Journal of Geophysical Research: Solid Earth*, *119*(10), 7654–7666. https://doi.org/10.1002/2014JB011307

Rosen, P. A., Gurrola, E., Sacco, G. F., & Zebker, H. (2012). The InSAR scientific computing environment [NTRS Author Affiliations: Jet Propulsion Lab., California Inst. of Tech., Stanford Univ. NTRS Document ID: 20150005896 NTRS Research Center: Jet Propulsion Laboratory (JPL)]. https://ntrs.nasa.gov/citations/20150005896

Ruiz, M. Z., Civilini, F., Ebinger, C. J., Oliva, S. J., Ruiz, M. C., Badi, G., La Femina, P. C., & Casas, J. A. (2022). Precursory signal detected for the 2018 Sierra Negra Volcanic eruption, Galápagos, using seismic ambient noise. *Journal of Geophysical Research: Solid Earth*, *127*(3), e2021JB022990. https://doi.org/10.1029/2021JB022990

Ruppert, N. A., Kozyreva, N. P., & Hansen, R. A. (2012). Review of crustal seismicity in the Aleutian Arc and implications for arc deformation. *Tectonophysics*, *522523*, 150–157. https://doi.org/10.1016/j.tecto.2011.11.024

Scuderi, M. M., Marone, C., Tinti, E., Di Stefano, G., & Collettini, C. (2016). Precursory changes in seismic velocity for the spectrum of earthquake failure modes. *Nature Geoscience*, *9*(99), 695–700. https://doi.org/10.1038/ngeo2775

Sens-Schönfelder, C., & Wegler, U. (2006). Passive image interferometry and seasonal variations of seismic velocities at Merapi Volcano, Indonesia. *Geophysical Research Letters*, *33*(21). https://doi.org/10.1029/2006GL027797

Sens-Schönfelder, C., Pomponi, E., & Peltier, A. (2014). Dynamics of Piton de la Fournaise volcano observed by passive image interferometry with multiple references. *Journal of Volcanology and Geothermal Research*, *276*, 32–45. https://doi.org/10.1016/j.jvolgeores.2014.02.012

Shen, Y., Ren, Y., Gao, H., & Savage, B. (2012). An improved method to extract verybroadband empirical greens functions from ambient seismic noise. *Bulletin of the Seismological Society of America*, *102*(4), 1872–1877. https://doi.org/10.1785/0120120023

U.S. Geological Survey. (2022). *ANSS Comprehensive Earthquake Catalog* (tech. rep.). U.S. Geological Survey. Menlo Park, CA.

Wang, J., Lu, Z., Bekaert, D., Marshak, C., Govorcin, M., Sangha, S., Kennedy, J., & Gregg, P. (2023). Along-arc volcanism in the western and central Aleutian from 2015 to 2021 revealed by cloud-based InSAR processing. *Geophysical Research Letters*, *50*, e2023GL106323. https://doi.org/10.1029/2023GL106323

Wang, J., Lu, Z., & Gregg, P. M. (2021). Inflation of Okmok Volcano during 20082020 from PS analyses and source inversion with finite element models. *Journal of Geophysical Research: Solid Earth*, *126*(10), e2021JB022420. https://doi.org/10.1029/2021JB022420

Wang, Q.-Y., Brenguier, F., Campillo, M., Lecointre, A., Takeda, T., & Aoki, Y. (2017). Seasonal crustal seismic velocity changes throughout Japan. *Journal of Geophysical Research: Solid Earth*, *122*(10), 7987–8002. https://doi.org/10.1002/2017JB014307

Waythomas, C. F., Miller, T. P., & Nye, C. (2003a). Preliminary geologic map of Great Sitkin Volcano, Alaska. *USGS Open-File Report*. https://doi.org/10.3133/ofr0336

Waythomas, C. F., Miller, T. P., & Nye, C. J. (2003b). Preliminary volcano-hazard assessment for Great Sitkin Volcano, Alaska. https://doi.org/10.3133/OFR03112

Wegler, U., Nakahara, H., Sens-Schönfelder, C., Korn, M., & Shiomi, K. (2009). Sudden drop of seismic velocity after the 2004 Mw 6.6 mid-Niigata earthquake, Japan, observed with passive image interferometry. *Journal of Geophysical Research: Solid Earth*, *114*(B6). https://doi.org/10.1029/2008JB005869

Xue, X., Freymueller, J., & Lu, Z. (2020). Modeling the posteruptive deformation at okmok based on the gps and insar time series: Changes in the shallow magma storage system. *Journal of Geophysical Research: Solid Earth*, *125*, e2019JB017801. https://doi.org/10.1029/2019JB017801

Yang, X., Bryan, J., Okubo, K., Jiang, C., Clements, T., & Denolle, M. A. (2022b). Optimal stacking of noise cross-correlation functions. *Geophysical Journal International*, *232*(3), 1600–1618. https://doi.org/10.1093/gji/ggac410

Yang, X., Roman, D. C., Haney, M., & Kupres, C. A. (2023). Double reservoirs imaged below Great Sitkin Volcano, Alaska, explain the migration of volcanic seismicity. *Geophysical Research Letters*, *50*(11), e2022GL102438. https://doi.org/10.1029/2022GL102438

Yang, X., Zuffoletti, I. D., D'Souza, N. J., & Denolle, M. A. (2022a, January). SeisGo: A ready-to-go Python toolbox for seismic data analysis. https://doi.org/10.5281/zenodo.5873724

Yuan, C., Bryan, J., & Denolle, M. (2021). Numerical comparison of time-, frequency- and wavelet-domain methods for coda wave interferometry. *Geophysical Journal International*, *226*(2), 828–846. https://doi.org/10.1093/gji/ggab140

Yunjun, Z., Fattahi, H., & Amelung, F. (2019, August). *Small baseline InSAR time series analysis: Unwrapping error correction and noise reduction*. https://doi.org/10.31223/osf.io/9sz6m